Progress in Retinal and Eye Research 107 (2025) 101378

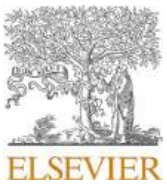

Contents lists available at ScienceDirect

Progress in Retinal and Eye Research

journal homepage: www.elsevier.com/locate/preteyeres

Widefield OCT angiography

Yali Jia [a,b,*], Tristan T. Hormel [a], Thomas S. Hwang [a], An-Lun Wu [a], Guangru B. Liang [a,b], Yukun Guo [a,b], Xiang Wei [a,b], Shuibin Ni [a], Yifan Jian [a,b], J. Peter Campbell [a], Steven T. Bailey [a], John C. Morrison [a], David Huang [a,b]

[a] Casey Eye Institute, Oregon Health and Science University, Portland, OR, USA
[b] Department of Biomedical Engineering, Oregon Health and Science University, Portland, OR, USA

ARTICLE INFO

Keywords:
Widefield imaging
Retina
OCT angiography

ABSTRACT

Optical coherence tomography angiography (OCTA) is a volumetric, non-invasive, high-resolution vascular imaging modality capable of acquiring highly detailed visualizations of retinal microvasculature. It has become an important tool for diagnosis and prognosis in prevalent diseases and pathologies such as diabetic retinopathy, retinopathy of prematurity, and vein occlusions, as well as more rare conditions, including inherited retinal dystrophies. It is also useful for measuring treatment response and assessing which patients would benefit from treatment. Unlike dye-based angiography, OCTA eliminates risks such as anaphylaxis. It also often outperforms fundus photography in feature detection. However, conventional OCTA imaging has been limited by its small field of view, which restricts simultaneous visualization of the posterior pole and peripheral retina, causing single images to potentially miss widely spaced critical biomarkers and pathological features. Recent technological advances in widefield OCTA have addressed this limitation, extending the field of view to the mid-periphery and beyond. This breakthrough enhances the simultaneous detection of macular and peripheral retinal pathology and significantly broadens OCTA's diagnostic and research applications. This review explores the technical innovations enabling widefield OCTA and highlights its clinical utility across various conditions, emphasizing its growing importance as a powerful tool in ophthalmic practice and research.

1. Introduction

Optical coherence tomography angiography (OCTA) combines several useful attributes for imaging the vascular anatomy of the eye. It can identify vessels down to the capillary scale in three dimensions and so can provide anatomically correct reconstructions of vascular morphology in the anterior segment, retina, and choroid. The images it captures compare well to histology (Balaratnasingam et al., 2019; Campbell et al., 2017c), but it has an additional advantage in that it can be applied *in vivo*. It is also a non-invasive imaging modality, which is advantageous with respect to the most established ophthalmic vascular imaging technology, dye-based angiography, which carries a low risk of adverse reactions and can be contraindicated for some patients for this reason (Bearelly et al., 2009; Kornblau and El-Annan, 2019; Xu et al., 2016). Achieving vascular imaging non-invasively is not the only advantage that OCTA obtains relative to dye-based angiography; from an imaging standpoint it has several other useful attributes. Due to improved resolution, OCTA is particularly effective for capturing small-scale pathology that dye-based angiography often cannot resolve, as we discuss below. Unlike dye injection technologies, OCTA does not rely on exogenous contrast agents, allowing it to avoid issues such as obscured vascular details caused by leaking vessels. The volumetric imaging capabilities of OCTA also contrast favorably with the two-dimensional images acquired with dye-based angiography. Furthermore, OCTA is less expensive, with procedures that are easier to perform than dye-based angiography (Swanson and Huang, 2011), which is an important advantage for clinical practice.

OCTA builds upon the foundation of structural OCT. Clinical adoption of structural OCT technology was driven by its ability to anatomically localize pathology like edema (Massin et al., 2003; Mookiah et al., 2015; Otani et al., 1999), retinal layer thinning (Leung et al., 2010; Wollstein et al., 2012), and exudation (Chen et al., 2012) which show up as either pathologic changes in retinal thickness or as fluid pockets. OCT can distinguish between different layers and identify fluid because these features have different reflectivity, which is a physical property of the materials. With other anatomic features, such as capillaries, this task is

* Corresponding author. Casey Eye Institute, Oregon Health and Science University, Portland, OR, USA
E-mail address: jiaya@ohsu.edu (Y. Jia).

https://doi.org/10.1016/j.preteyeres.2025.101378
Received 21 January 2025; Received in revised form 6 June 2025; Accepted 10 June 2025
Available online 13 June 2025
1350-9462/© 2025 Elsevier Ltd. All rights are reserved, including those for text and data mining, AI training, and similar technologies.

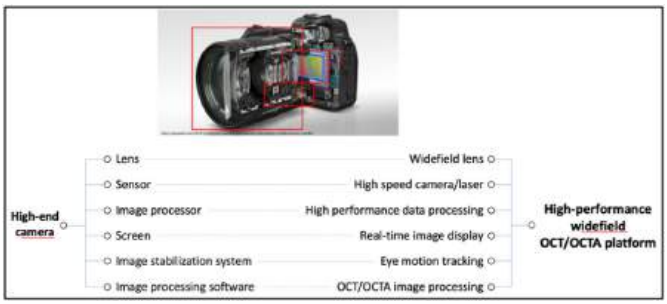

Fig. 1. *Widefield OCTA analogy with a camera, component by component. In* widefield *OCTA, many of the hardware components have analogies to image capture with a high-end camera, as shown in the table here.*

more difficult because their reflectivity is more similar to the surrounding tissue. Furthermore, structural OCT cannot reveal functional information such as blood flow. This is unfortunate because it limits structural OCT's ability to detect microvascular changes and how they relate to retinal structure and function (Iadecola, 2017; Scanlon, 2019).

OCTA processing leverages motion contrast instead of reflectance to both more readily visualize microvasculature and indicate the presence of flow. The basic idea is to capture sequential structural OCT cross-sections and compare the speckle difference caused by erythrocyte movement. The signal originating from this difference is called the "flow signal". Thus, motion contrast becomes an endogenous contrast agent that allows the differentiation of static and vascular tissue. OCTA also inherits the major advantages of structural OCT imaging (i.e., non-invasiveness, depth-resolution, high-resolution, and ease of use). These capabilities have positioned OCTA as a valuable tool in basic, translational, and clinical research, and it is also being increasingly adopted in clinical practice.

Nonetheless, OCTA is not a panacea for retinal vascular imaging. Importantly, in many commercial instruments, and in most studies and clinical practice, it captures fields of view that are relatively limited compared to allied imaging modalities such as fundus photography and dye-based angiography. With restricted fields of view like these either peripheral or macular features can be captured, but not both. Consequently, some important pathologic features may be missed. To give just one example, peripheral ischemia is closely associated with disease progression and treatment response in multiple diseases (Quinn et al., 2019). Since conventional OCTA imaging usually captures only the posterior pole this feature would be missed. This underscores the critical importance of OCTA with a wide field of view, particularly for vascular

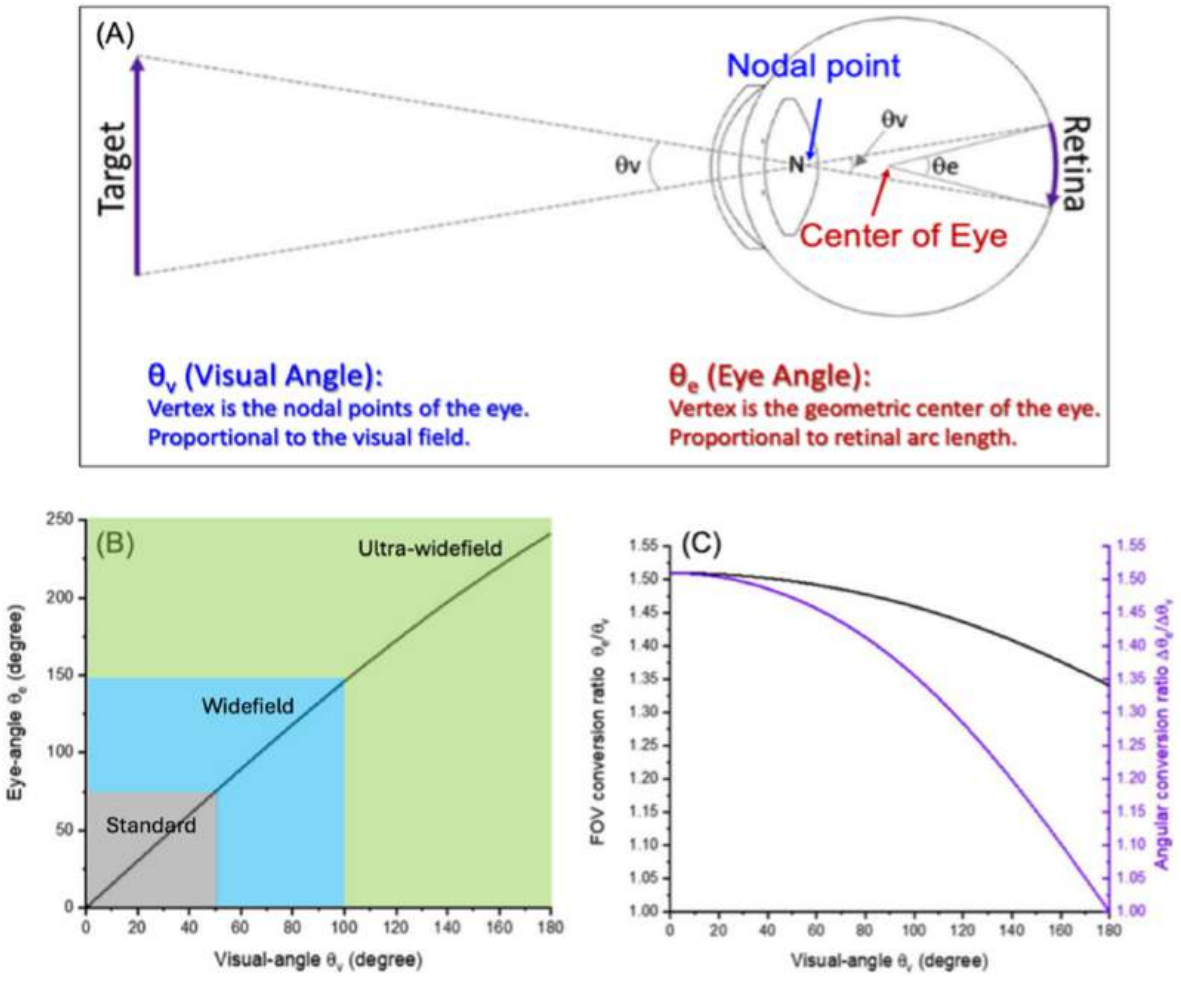

Fig. 2. Visual angle and eye angle. The field of view in OCTA is often defined using one of two different angles inscribed on two idealized circles. (A) The visual angle θ_v uses the nodal point on the eye's pupil as the angle vertex, while the eye angle θ_e uses the center of the eye as the vertex. Both can describe the field of view. Note that since the eye angle is linearly proportional to the arc length of the retina, peripheral pixels will have larger physical transverse width than central. (B) Visual angle vs. eye-angle over 180 degrees of the visual angle. The shaded regions and showing standard, widefield, and ultra-widefield correspond to the definitions given in Table 1. (C) Conversion between visual and eye angle changes based on the total visual (or eye) angle. The field of view ratio (θ_e/θ_v) decreases as the visual angle increases. Another way to consider changing between the two is how much the eye angle changes with a small change in visual angle, $\Delta\theta_e/\Delta\theta_v$. This quantity more rapidly decreases with visual angle, reaching unity at 180°. With permission from (Yao et al., 2021).

diseases that originate in or predominantly affect the peripheral retina. In this review, we will discuss how to achieve wider fields of view with OCTA and the clinical advantages of doing so.

2. Technical concerns for extending the field of view

2.1. Primer

There are two non-exclusive approaches to extending the field of view in an OCTA device. The first involves capturing multiple images and stitching them together to create a composite image, a process known as montage. The second approach captures a wider field of view in a single volume, referred to as single-shot imaging.

The major technical consideration for montaged OCTA is the ability to stitch images together. There are many approaches for accomplishing this (Cheng et al., 2021; Hendargo et al., 2013; Mase et al., 2016; Niederleithner et al., 2023; Wang et al., 2019). Although some early OCTA studies captured wide fields of view using over ten smaller volumes to produce a montaged image (e.g. (Mase et al., 2016)), this approach is not practical for clinical imaging due to the complexity and time requirements of such a procedure. Contemporary montage approaches consequently usually rely on over 100-degree imaging and employ montage techniques to further extend the field of view (Niederleithner et al., 2023).

Expanding a single-shot field of view in OCTA involves several critical factors, as illustrated in Fig. 1, which compares these factors to the more familiar configuration of a high-end camera. Among these, imaging speed (represented by a high-speed camera/laser combination) is perhaps the most important. Most widefield systems rely on swept-source OCT (SS-OCT) technology, which is the current standard bearer for rapid OCT imaging (Huang et al., 2020; Kang et al., 2018; Wang et al., 2023a). SS-OCT requires lasers capable of rapidly modulating their wavelength, along with high-speed signal detection and digitization (Section 2.2). Additionally, to image peripheral regions clearly without introducing vignetting artifacts, careful attention to system optical design is essential (Section 2.3). Efficient and sensitive OCTA data processing can also help image vasculature in detail and reduce procedure time (Section 2.4). The living eye is not a static system, and eye motion during image acquisition is common, if not inevitable. Since OCTA depends on motion contrast, effective tracking and motion correction are critical components of a successful system (Section 2.5). Even with these advancements, widefield OCTA imaging takes longer than conventional OCTA. As a result, ensuring robust quality control through real-time display during data acquisition is vital to make widefield OCTA viable for clinical use (Section 2.6). Together, these innovations bring us closer to realizing the full potential of widefield OCTA for comprehensive retinal imaging. First, though, we will discuss what "widefield OCTA" means.

2.2. Defining "widefield"

What constitutes "widefield" OCTA? Unfortunately, the term isn't used consistently among researchers. Similarly, attempts to reach consensus among the research community have so far been unsuccessful, with multiple studies proposing different boundaries for widefield images (Choudhry et al., 2019; Munk et al., 2022; Pichi et al., 2021). It should be noted that amongst these studies, Choudhry et al. was an attempt to define the term across multiple imaging modalities, while Munk et al. focused on just OCTA, and the Pichi study considered just OCTA imaging in uveitis. This may account for some of the disagreement. Even within an individual study Munk et al. noted that some of the experts in their Delphi approach had misgivings about the final recommendations.

Part of the difficulty lies in describing the dimensions of a retinal image. One approach is to define the lateral dimensions of the image (length × width) on the retinal surface: 3 × 3-mm, 6 × 6-mm, 12 × 12-mm, 12 × 23-mm, etc. The problem with this approach is that actual physical dimensions of the field of view depend on the axial length of the eye being imaged, which may not be known. Furthermore, the real lateral dimensions would vary depending on the eye being imaged even with the same scanning protocol. As an alternative, we can consider using the angular coverage. However, this approach has an important ambiguity concerning the choice of the angle vertex. There are two common choices (Fig. 2). The eye angle is taken from the center of the eye while the visual angle (or scanning angle) is taken from the nodal point for instrument scanning. These two angles are non-linearly related (Fig. 2B and C). One reason "widefield" is not used consistently defined is that all three of these metrics (lateral dimensions, eye angle, and visual angle) can be found in the literature.

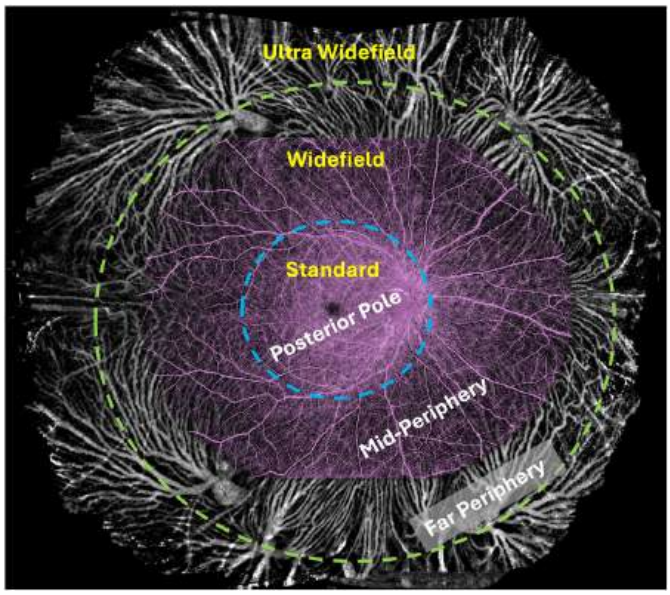

Fig. 3. Widefield OCTA terminology. Anatomic definitions are given in white lettering, while suggested instrument field of views are shown in yellow lettering. Here, "widefield" corresponds to the region between the blue and green dotted lines, while ultra-widefield corresponds to the region beyond the green dotted line. The purple highlight gives the field of view achieved by a contemporary widefield OCTA enabled device (Intalight DREAM). Note that this definition of ultra-widefield is not achievable with most contemporary devices without the use of montage. (For interpretation of the references to color in this figure legend, the reader is referred to the Web version of this article.)

Another reason that "widefield" isn't consistently defined relates to context. The studies we cited above come from academia, but instrument manufacturers also provide their own definitions of a widefield scan. Also, the terms themselves have evolved over time as the fields of view in OCTA imaging increase. This means that in some early studies 12 × 12-mm or even 6 × 6-mm images may be called "widefield". The current review takes the view that these images are too small to be considered widefield.

Last, we note that in addition to the term "widefield," "ultra-widefield" is also frequently encountered in the literature. This term encounters all of the same ambiguities in usage as "widefield".

All of this may seem like semantics but precise definitions of the field of view are critical for quantifying pathology in widefield imaging, and for comparing the performance of various devices. For example, a 30 % reduction in perfused tissue is a much larger area if we are talking about a 26 × 21-mm widefield image than if we are talking a 12 × 12-mm widefield image. There is a need for this terminology to be established.

In the current work we define "widefield" and "ultra-widefield" by appealing to retinal anatomy, similar to the approach taken by Choudhry et al. (2019). Using retinal anatomy for inspiration helps to

Table 1
OCT angiography field of view definitions. These definitions are based on anatomy, with widefield encompassing the mid-periphery and ultra-widefield extending to the far periphery.

	Eye Angle	Visual Angle
Widefield	75°	50°
Ultra-widefield	146°	100°

build an intuition for the types of features that could be captured by a specific field of view. But it lacks the rigor of a mathematical boundary. We therefore choose to define "widefield" as capturing at least the posterior pole and extending through the mid-periphery to the vortex veins, while "ultra-widefield" imaging is any larger field of view covering the far periphery (Fig. 3). The corresponding eye and visual angles are given in Table 1.

2.3. Improving Scan acquisition rate

OCTA image acquisition cannot occur over arbitrarily long time periods. Over long time frames sources of motion including bulk eye motion, ocular pulsation and drift, and saccade will eventually overwhelm motion contrast due to blood flow and obscure the flow signal to the point that it can no longer be extracted using the OCTA approach. Therefore, improvements in scan acquisition rate are among the most important innovations enabling widefield OCTA imaging. Larger images have more sampling points than smaller, and by increasing acquisition rate we can extend the field of view without approaching unviable scan durations.

Before we continue this discussion it should be noted that OCTA studies are not always careful about terminology since there are A-scan, B-scans, C-scans, and volume scans all being discussed. In the following we by "scan acquisition" we mean A-scan acquisition, while for the total volume we say "image acquisition". Image acquisition rate depends on both the size of the field of view being acquired and the sampling density within that field of view and is consequently not a convenient metric for assessing OCTA system speed. Alternatively, scan acquisition rate only concerns the time it takes to complete an A-scan and so can be more easily compared across devices.

The fastest OCTA systems today use swept-source lasers that can achieve megahertz sweep rates. This sweep rate is usually rate limiting for A-line acquisition in OCTA. Fourier domain mode-locking (FDML) was an important innovation for this purpose (Gorczynska et al., 2017; Huber et al., 2006; Klein et al., 2011; Wieser et al., 2010). Microelectromechanical system (MEMS) vertical cavity surface emitting laser (VCSEL) systems can achieve similar sweep rates while increasing coherence length and have demonstrated lower signal roll-off, which is important for posterior retinal and choroidal imaging (Chen et al., 2022; John et al., 2015; Potsaid et al., 2012; Zhang et al., 2021). Most recently stretched-pulse mode-locking (SPML) systems have achieved scanning rates in the 10's of MHz (Akkaya and Tozburun, 2022; Wang et al., 2023b), although these devices haven't demonstrated OCTA. SPML illumination relies on dispersive media rather than mechanical wavelength scanning (as in FDML and VCSEL sources), which can enable such rapid sweep rates (Tozburun et al., 2014).

OCTA systems must also sample and digitize the interference spectrum generated by the device in order to produce images. The rate at which we can sample the interference spectrum determines how many pixels we can include in a line scan, which makes rapid/accurate sampling critical for extending imaging depth. Imaging depth itself is also important for widefield imaging, where it can be the feature that limits the widest achievable imaging angle. In SS-OCTA, sampling is performed in *k*-space because wavelength and depth form a Fourier transform pair. We would like to sample this space linearly (Wojtkowski et al., 2002), but swept-source laser sweep rate is not typically uniform so if we sample at regular time intervals, we will not get a linear-in-*k* interferogram. To counteract this effect, optically generated timing references created using the swept-source laser output can be used to ensure that sampling is linear-in-*k*. Common choices to achieve this are to optically couple the swept-source laser to a Fabry-Perot (Choma et al., 2005), Mach-Zehnder (MZI) (Chen et al., 2022; Xi et al., 2010; Zhang et al., 2004) or Michelson interferometers (Potsaid et al., 2010). These approaches have demonstrated high performance clocking, but they cannot fully utilize digitizer rates (Attendu and Ruis, 2019; Chen et al., 2022; Zhang et al., 2021) and can suffer signal degradation due to signal timing mismatch (Moon and Chen, 2018). The other option is to numerically resample the OCT signal (Yasuno et al., 2007). Many established signal processing methods have been applied to OCT to obtain a uniform *k*-spacing including linear or spline interpolation and convolution. In a head-to-head comparison that also included non-uniform signal reconstruction techniques, Vergnole et al. found that convolutional resampling and reconstruction achieved the best results (Vergnole et al., 2010). The issue with these methods is that in sacrificing sweep calibration they will usually sacrifice axial resolution to phase instability (Potsaid et al., 2010). In modern systems, numerical polynomial fitting after an initial phase calibration can be used for *k*-clocking and achieve both high resolution and depth penetration (Huang et al., 2024).

Rapid OCTA acquisition also relies heavily on performances of laser scanners, which drive the beam point by point across the imaging field. The most utilized laser scanners used in OCTA are galvanometer-based scanners (GS), thanks to their large scanning angles, precise positioning, accessible control frequency, manageable compactness, and reasonable cost. However, at large scanning angles, the scanning speed is limited due to the mechanical inertia of the GS (Duma et al., 2015). This limitation is particularly evident in the currently most employed unidirectional scanning method, where a portion of scanning time is lost to flyback, which is needed to compensate for the GS's response time. This inefficient use of scanning time presents a challenge to further increase imaging speeds. Additionally, the fast A-scan rate provided by advanced laser will lead to a shorter interscan time which will reduce the OCTA flow sensitivity to slow flow. While a simple bidirectional scanning pattern offers a high duty cycle and reduces mechanical stress on the GS (Duma et al., 2015, 2011), the varying interscan time intervals it produces are unsuitable for OCTA (Ju et al., 2018). Instead, a bidirectional interleaved scanning protocol with an adjustable number of positions in the slow-axis positions within one repeating unit can sustain the optimal time delay for OCTA generation even with a high A-scan rate (Wei et al., 2019a).

Both scanning density and field of view can be increased with a faster scanning rate. For the scanning density we can identify a limit based on the sample beam size beyond which improving scanning density does not yield novel information-we end up just resampling information we already have. But if we adhere to this limit-the Nyquist limit-while expanding the field of view, even with the swiftest illumination sources the entire field of view may not be very large. Instead, it is often convenient to undersample by reducing the scanning density below the Nyquist limit. This lowers image resolution, but in many cases this can be acceptable: if we are just looking for non-perfusion area, for example, we need only ensure that we have sufficient resolution to detect capillaries. On the other hand, denser scanning patterns may be required for detecting flow deficits on the choriocapillaris or other small-scale features such as microaneurysms. Most commercial devices have multiple scan protocols for this reason.

2.4. Optical considerations

Widefield OCTA imaging may require more complicated optical setups than for conventional 3 × 3- or 6 × 6-mm fields of view in order to image peripheral or deep tissues at high resolution while avoiding artifacts. A key concern is the achievable scanning angle, which determines the extent of the retina that can be sampled by system. A

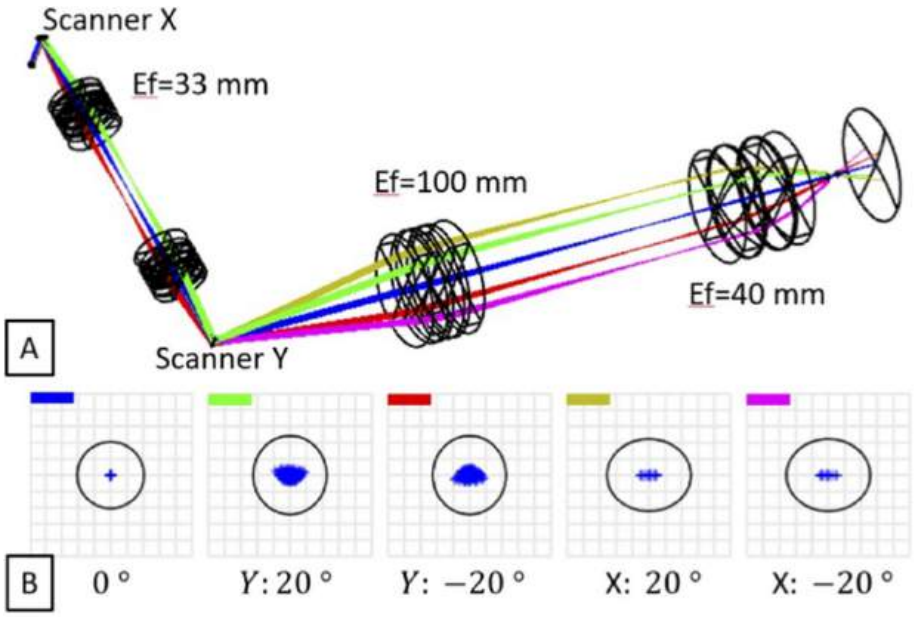

Fig. 4. Sample arm optical configuration for widefield OCTA. (A) Schematic of the OCT sample arm with optical relay, with effective focal length Ef. Different color rays denote different scanning angles. (B) Spot diagrams of five different scanning angles, simulated in OpticStudio (Zemax, LLC). The color bar at the top left of each diagram corresponds to the ray colors in (A). With permission from (Wei et al., 2019c). (For interpretation of the references to color in this figure legend, the reader is referred to the Web version of this article.)

common approach for expanding the scanning angle is a 4f lens system (Kolb et al., 2015; Liang et al., 2023; Niederleithner et al., 2023; Wei et al., 2019c). These systems contain two lens groups that are symmetrically configured and can achieve two desirable features for widefield OCTA imaging. First, they increase the scanning angle by a factor of the ratio of the effective focal lengths of the lens groups. Second, they produce a scanning pivot point on the sample which is useful for imaging through the pupil. Asymmetric configurations are sometimes used to help compensate for aberrations (Liang et al., 2024; Ni et al., 2021).

Vignetting is a larger concern in widefield imaging than in conventional OCTA. It can be caused by the pupil blocking the probe beam (mydriasis can help with this), or by misalignment between the system and eye. In particular, OCTA alignment often relies on paired GSs to adjust scanning location along the slow and fast axes. Since the GSs are separate components their axial focal points are not necessarily aligned, which can lead to vignetting. To counter this effect an optical relay (Fig. 4), that may also rely on a 4f-lens system, can be employed to map the fast scan signal on to the slow scan (Wei et al., 2019c).

Signal attenuation effects are another important consideration in OCTA. Signal attenuation effects can originate from pathologic features (e.g. vitreous floaters or retinal fluid) or instrument misalignment (defocus or vignetting). These effects are local, which means they are exacerbated in widefield imaging: signal strength will typically vary more across a larger field of view than a smaller, and is usually more extreme in peripheral regions of the image. OCTA signal processing should account for this. OCTA metrics should also consider the effects of

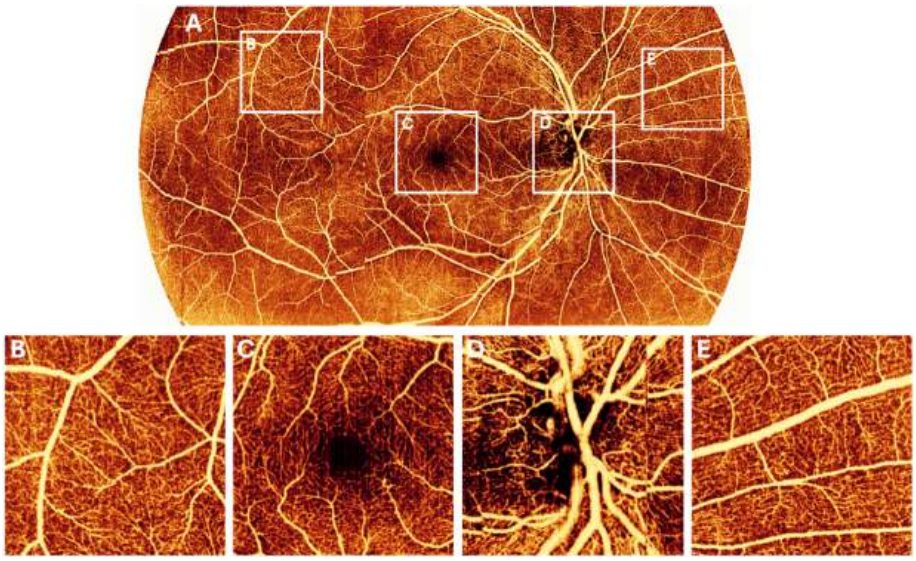

Fig. 5. A widefield OCTA image acquired from a healthy subject using a phase-stabilized complex-decorrelation OCTA processing algorithm. With appropriate hardware, images like this can be generated in real-time during scan acquisition. (A) 12 × 23-mm widefield PSCD OCTA image, (B–E) zoomed localized images cropped from (A). With permission from (Wei et al., 2021).

signal attenuation; this can be accomplished by explicitly considering these effects in algorithm development (Guo et al., 2019; Nesper and Fawzi, 2022), by using measurements less prone to corruption by signal loss (i.e. choosing non-perfusion area measurements over vessel density measurements (Hwang et al., 2018; Xiong et al., 2021)) or by excluding severely affected areas (Camino et al., 2019; Guo et al., 2019).

2.5. OCTA data processing

OCTA imaging is an interferometric imaging approach. Interferometric signals contain both amplitude and phase components and the differences between either or both can be used to construct the OCTA signal. Phase-based processing produced the first recognizable OCTA images (Makita et al., 2006). But phase-based approaches are sensitive to phase noise which requires a phase compensation approach, of which there are several (Liu et al., 2016; Miao et al., 2021; Moon and Chen, 2018; Poddar et al., 2014; Schwartz et al., 2014). Phase correction is not necessary in amplitude-based approaches which makes them simpler to implement (Jia et al., 2012). Complex-based approaches also require phase stabilization. However, using both the phase and amplitude portions of the interferometric signal means that all the available information is being considered (An and Wang, 2008).

An important aspect of OCTA data generation is the number of repeat scans required to construct the image, with the theoretical minimum being two. Efficient algorithms can significantly reduce scanning time, such as the spectral splitting approach, which averages signals over subbands to enhance the signal-to-noise ratio for flow detection (Jia et al., 2012; Liu et al., 2016). Another method involves improving OCTA signal sensitivity by integrating both amplitude and phase components, supported by a highly precise phase bulk motion compensation technique (Wei et al., 2021) (Fig. 5). Efficient algorithms like these are especially important in widefield imaging because it takes longer to collect a full volume scan. In OCTA we already need to do this at least twice to produce motion contrast; tripling or quadrupling the number of scan volumes is a more serious problem when scan acquisition is relatively time consuming. For research devices that are not as constrained by patient throughput, this can sometimes still be a good trade-off and more than two repeats can be used even with efficient OCTA generation algorithms to improve image quality (Zhang et al., 2016).

Efficient OCTA signal generation can help improve flow detection sensitivity. The flow signal itself though is physiological in origin. Its magnitude as measured by OCTA is determined by both this physiological substrate which includes blood flow speed and vessel caliber (as well as some other features such as erythrocyte density or anterior opacities) (Su et al., 2016; Yang et al., 2017b). Both vessel caliber and blood flow speed vary with retinal anatomic location (Feke et al., 1989). For example, blood flow speed is slower in the periphery than in the macula. It can also be slowed due to some pathologic conditions (Arya et al., 2021; Forte et al., 2025; Rebhun et al., 2017). This might imply that OCTA could lose detection sensitivity in peripheral regions, but flow signal magnitude is also dependent on measurement parameters (including the signal generation algorithm and hardware sensitivity). A measurement parameter available to any device is interscan time, which can be adjusted through changes in the scan pattern. Longer interscan times can detect slower flow, but the trade-off is that the flow signal will saturate for higher flow speeds, meaning we can't differentiate flow magnitude in large vessels or other vessels with swift flow (Su et al., 2016). One way to measure both is to make use of both long and short interscan times using multiple repeat B-scans. High-dynamic range OCTA (HDR-OCTA) uses several interscan times with an efficient scanning pattern to extend the dynamic range for flow detection in OCTA (Wei et al., 2019d). Flow detection in peripheral regions could benefit from this or similar approaches.

After generating the flow signal, additional image processing steps are typically applied to enhance image quality. Image enhancement focuses on reducing noise and highlighting relevant features, such as vessels. Traditional methods, like vesselness filters, are often used but have limitations: they require manual design and can create false vessels due to a lack of anatomical context. Artificial intelligence (AI) addresses these issues by learning anatomical context, and consequently delivering superior results (Hormel et al., 2021a). Conventional AI training requires a ground truth to learn from, which is subtle when we don't have access to the real anatomic configuration of the eye to compare to. One approach is super-resolution reconstruction, in which high-resolution scans from the same region as a low-resolution scan serve as the ground truth, allowing the network to upscale resolution (Gao et al., 2020). (Notably, this network also improved the high-resolution images used in training.) Similarly, scan volumes constructed from more repeats (i.e. with less noise) can train networks to enhance/denoise scans constructed from fewer repeats (Abu-Qamar et al., 2023; Gao et al., 2021). These advanced AI-driven techniques are now entering clinical practice, as demonstrated by devices like the Intalight DREAM OCT.

Artifacts, such as vignetting, motion, and projection artifacts, are also addressed through image processing. Projection artifacts are not unique to widefield OCTA. Their origin, and methods to address them, are discussed extensively in our previous review article (Hormel et al., 2021b). Motion artifacts are particularly significant in widefield OCTA and demand specialized solutions, which we will discuss now.

A near-ubiquitous data processing step in OCTA is layer segmentation. Layer segmentation is required to produce *en face* images, which are the most common way to analyze OCTA data by a substantial margin. Layer segmentation is a time-consuming task in OCTA. Several strategies to complete this task have been covered extensively in other recent reviews (Hormel et al., 2021a; 2021b). With widefield imaging the task is compounded by the disparity between retinal structure in the periphery and macula. For example, some layers and plexuses merge in the periphery. Furthermore, the optic nerve head is an especially difficult structure for layer segmentation in comparison to the rest of the retina. For this reason, multiple layer segmentation strategies may be necessary to cover each of these different anatomic locations. Even in small fields of view manual layer segmentation correction may be needed when pathologic features such as retinal fluid are present. This remains an option with wider fields of view but becomes correspondingly more difficult and time consuming. Effective layer segmentation for widefield imaging remains an active area of research.

An option step for widefield imaging is correcting for image distortion. A well-known result from cartography states that we cannot simultaneously preserve area and shape when projecting a curved surface on to a flat one. (This is why Greenland looks so over-sized in the Mercader projection.) A similar problem occurs with OCTA *en face* images, which must necessarily be spatially or morphologically distorted (or both). What this means is that the real lateral dimensions of a pixel in an OCTA image will vary across the field of view as we project a curved surface on to a flat screen. This is an issue that is aggravated in widefield imaging: distortive effects in small fields of view are not as extreme. Distortion can be controlled using image transformations, but it cannot be eliminated altogether (Mehta et al., 2021; Tan et al., 2021; Westphal et al., 2000). One way to account for this effect is to use metrics composed of ratios (vessel density and flow deficit ratio are two examples). This approach avoids the issues altogether since any distortions will be cancelled out by the ratioed metric.

2.6. Motion tracking and motion correction

In extended fields of view, eye motion becomes more relevant. This is because even the fastest available systems have thus far not proven capable of image acquisition times swift enough to overcome processes like saccade, ocular pulsation, and drift (Ditchburn and Ginsborg, 1953). Given that widefield scanning increases imaging times, these effects cannot be ignored. There are two overlapping approaches to dealing with motion. The first is motion tracking, in which we continually

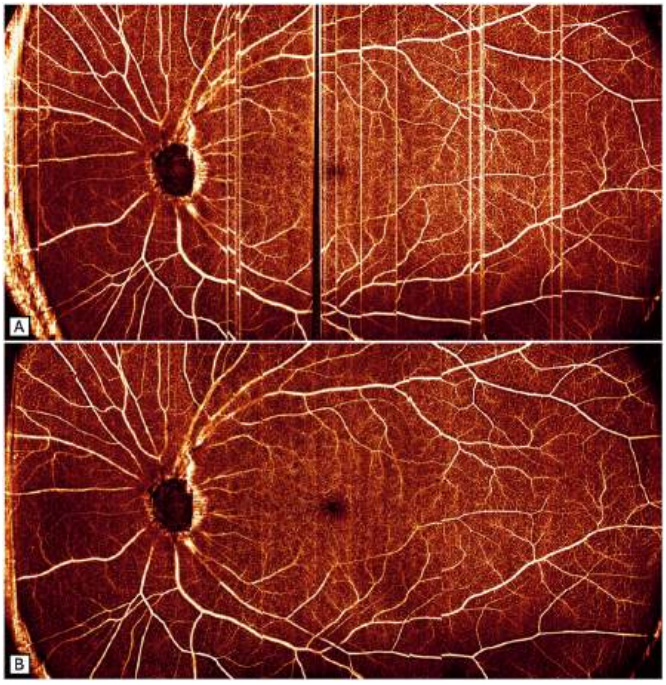

Fig. 6. ***Removal of motion artifacts using a self-navigated motion correction approach.*** *(A) 12 × 23-mm widefield OCTA image acquired without self-navigated motion correction engaged; (B) widefield OCTA image acquired with self-navigated motion correction engaged.* Images were captured with a. lab-built prototype. With permission from (Wei et al., 2020).

re-align the system optics during an imaging procedure in order to follow along with eye movement. The second is motion correction, which often relies on image registration, where we attempt to remove motion-induced artifacts from an acquired image. These approaches are complementary and using them in conjunction can improve image quality (Camino et al., 2016).

A popular means of tracking eye motion in OCTA is to use allied imaging modalities such as scanning laser ophthalmoscopy (Braaf et al., 2013), line scan ophthalmoscope (Zhang et al., 2015, 2016) or infrared camera (Camino et al., 2016). In these approaches, the allied imaging modalities provide rapid imaging that can be used to track eye motion and adjust scan patterns in order to accommodate drift or other eye movements. One important limitation of such a scheme is that because the allied modalities are not depth-resolved, we cannot ascertain if axial motion is still present. This type of tracking is also most effective in regions with large vessels (e.g. the peripapillary) in which fiducial markers are available. This means that they may experience performance loss in regions like the macula where such prominent anatomic features are unavailable. This is a problem especially for infrared cameras, the cheapest approach. This relates to another issue: the hardware becomes more complex and expensive by relying on a supporting imaging modality. It is natural to ask if it would be possible to achieve motion tracking that relies on just OCTA. A conceptually simple but effective way to achieve this is self-navigated motion correction (Fig. 6), in which the device will rescan problematic regions in which motion artifacts are especially severe (Wei et al., 2020). The "self-navigation" aspect of this solution is that the system will rescan after microsaccade or other disruptions once the eye has returned to the fixational position. This means that self-navigation is a passive tracking approach. If we want to use only OCTA for motion tracking, we also need to do the OCTA processing in real time, which is a non-trivial engineering task we will discuss below.

In addition to tracking, we can also use motion artifact correction, which often relies on image registration. Image registration is a well-studied problem in image analysis (Zitová and Flusser, 2003). In conventional OCTA with small fields of view motion artifacts can often be removed by registering X-fast and Y-fast scan volumes (that is, scans collected with the fast direction along orthogonal axes) (Ploner et al., 2021; Zang et al., 2017). However, in widefield imaging, volume scan acquisition will take too long for this approach to work well because the X-fast and Y-fast scans come out of alignment, making the registration task much more difficult. Note also that registration approaches like these rely on multiple volume acquisitions (i.e. X-fast and Y-fast OCTA) in order to prevent loss of information in regions where information is not recoverable (for example during a blink). Instead, we can register along parallel strips within the scan volume, dividing the registration task into smaller and more manageable sub-regions (Zang et al., 2016). This can also be accomplished volumetrically (Fig. 7) (Zang et al., 2017).

While there is a large amount of literature concerning image registration, In OCTA we have a relatively niche application since we care about three-dimensional registration, whereas the vast majority of research concerns two dimensional images. (OCTA data can, of course, be registered at the *en face* level.) Probably the most problematic aspect of image registration in OCTA is the varying signal quality between separate acquisitions. This can exacerbate the effect of local signal attenuation. This effect is basically unavoidable; the best we can do is to ensure that our algorithms are resilient to changes in signal strength. Furthermore, even with the most sophisticated image registration methods we some distortion of the vascular anatomy may occur.

Not all motion correction relies on image registration. Because OCTA uses motion contrast to detect flow background, sources of motion such as drift can manifest as background. An efficient way to remove this background is with an iterative approach based on regression that estimates and then subtracts the bulk motion contribution to the signal (Camino et al., 2017, 2018).

2.7. OCTA in real-time

As we discussed above, the scan speed can be improved using swept-source illumination. Another relevant speed in OCTA is data processing speed. OCTA images are usually processed after acquisition. The problem with this solution is that we cannot assess image quality during acquisition. This means that we may have acquired a low-quality scan unsuitable for analysis when operator feedback could have allowed us to acquire a high-quality scan. Ultimately this reduces efficiency and therefore clinical throughput. The alternative is to process OCTA in real time.

Real-time OCTA is achieved through two main strategies: efficient signal processing and reduced computation complexity. Efficient signal processing typically relies on graphic processing units (GPUs), as demonstrated in early implementations (Lee et al., 2012). Making judicious use of device threads, for example by dividing structural OCT and OCTA generation, can help boost performance (Wei et al., 2019b). The other important method for achieving real-time OCTA is reducing OCTA computation complexity. This can be accomplished by using simpler algorithms like speckle variance (Lee et al., 2012; Xu et al., 2014), though this may come at the cost of image quality.

Defocusing, vignetting, and bulk motion degrade the image quality in OCTA more significantly than structural OCT. Nonetheless the assessment of focus, alignment conditions, and stability of imaging subjects in commercially available OCTA systems are currently based on OCT signal quality alone, without knowledge of OCTA signal quality. This results in low yield rates for further quantification. Real-time OCTA generation can improve the situation by allowing system operators to assess the presence of artifacts during scan acquisition, but since key artifacts like vignetting or shadowing are more apparent in OCTA *en face* images, we may also need to form *en face* images in real time. This means that we need real-time layer segmentation, which is only feasible for whole retina images (which rely on relatively simple segmentations of the inner limiting and Bruch's membranes). Even barring real-time data display though real-time OCTA remains useful because the flow signal is

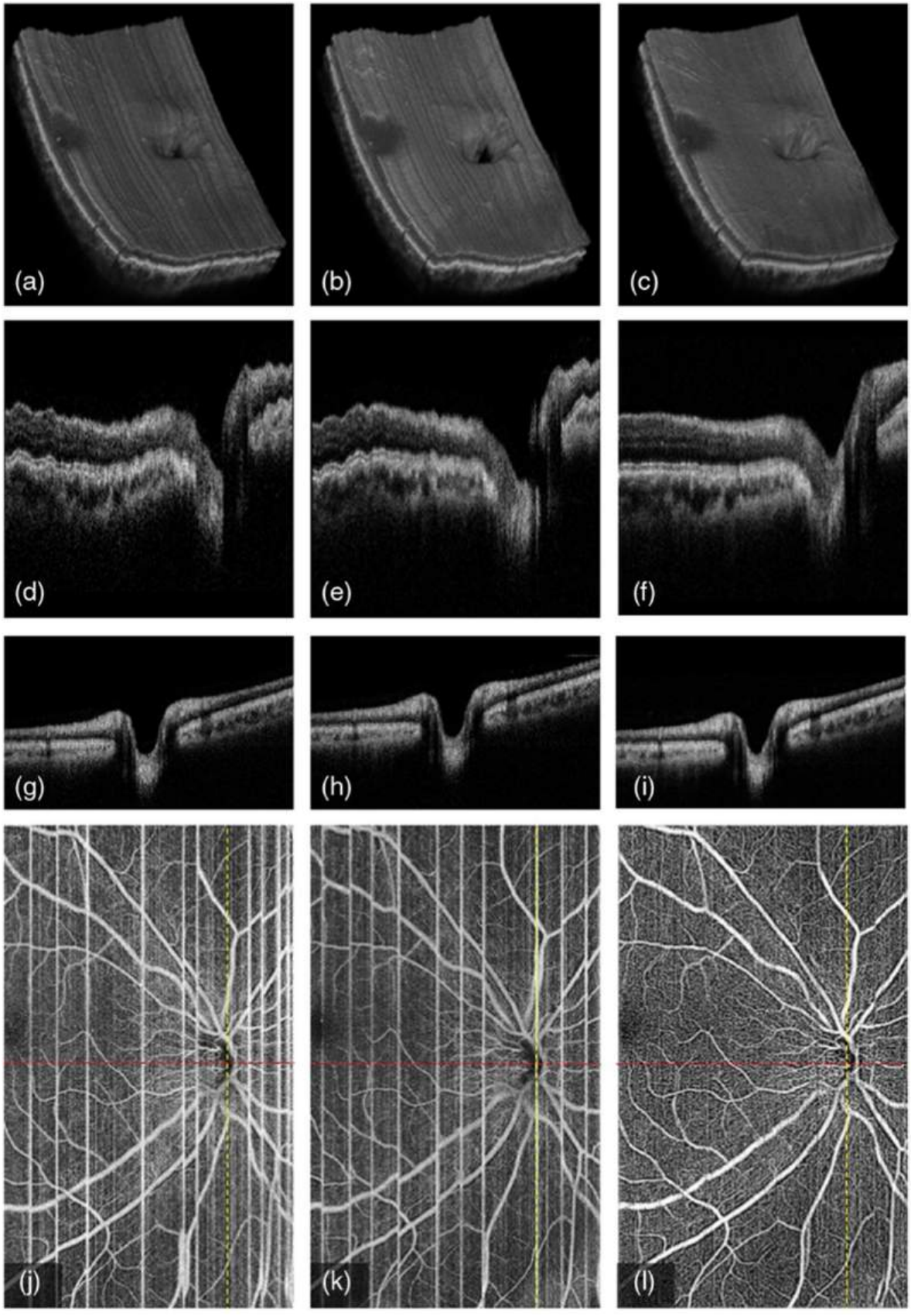

(caption on next page)

Fig. 7. 3-D registration of two Y-fast volumetric OCT and OCTA (6 × 10 × 7 -mm) of the disc region on a normal eye. (a) first volumetric OCT, (b) second volumetric OCT, (c) merged volumetric OCT after the 3-D registration of a and b, (d) the B-frame along X (slow)-axis in first volume (red line in j), (e) the B-frame along X-axis in second volume (red line in k), (f) the B-frame along X-axis in the merged volume (red line in l), (g) the B-frame along Y (fast)-axis in first volume (yellow line in j), (h) the B-frame along Y-axis in second volume (yellow line in k), (i) the B-frame along Y-axis in the merged volume (yellow line in l), (j) first en face OCTA, (k) second en face OCTA, and (l) the merged en face OCTA after 3-D registration of two volumes. In this algorithm, A-scans are first transversely aligned within a B-scan (d-i), following which axial motion is corrected along the boundary of the inner limiting membrane. Within frame registration yields local optimization. This non-orthogonal image registration algorithm is suitable for widefield imaging. With permission from Zang et al. (Zang et al., 2017). (For interpretation of the references to color in this figure legend, the reader is referred to the Web version of this article.)

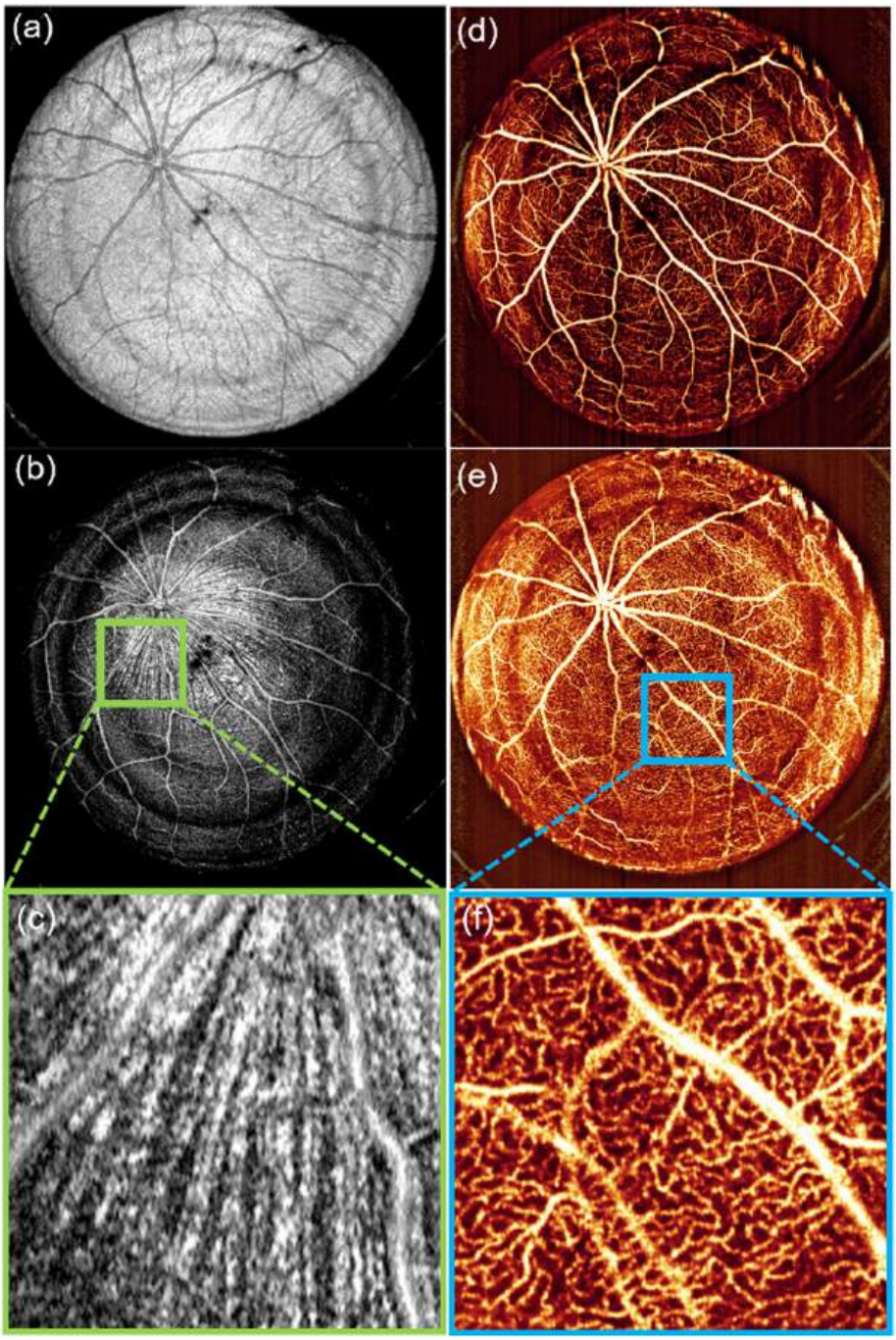

Fig. 8. 112° visual angle high resolution en face retinal images of a mature, healthy Brown Norway rat taken with a lab-built device. (a) OCT projection of the whole retina, exemplifying the large FOV that can be achieved. (b) OCT projection of the nerve fiber layer. (c) Cropped images from the highlighted region in (b), with clear differentiation of individual nerve fiber bundles, demonstrating the high lateral resolution achieved by the system. (d) OCTA projection of the superficial vascular layer. (e) OCTA projection of the deep vascular layer. (f) Cropped images from the highlighted region in (e), showing detailed capillaries with their lobular nature. With permission from (Liang et al., 2024). (For interpretation of the references to color in this figure legend, the reader is referred to the Web version of this article.)

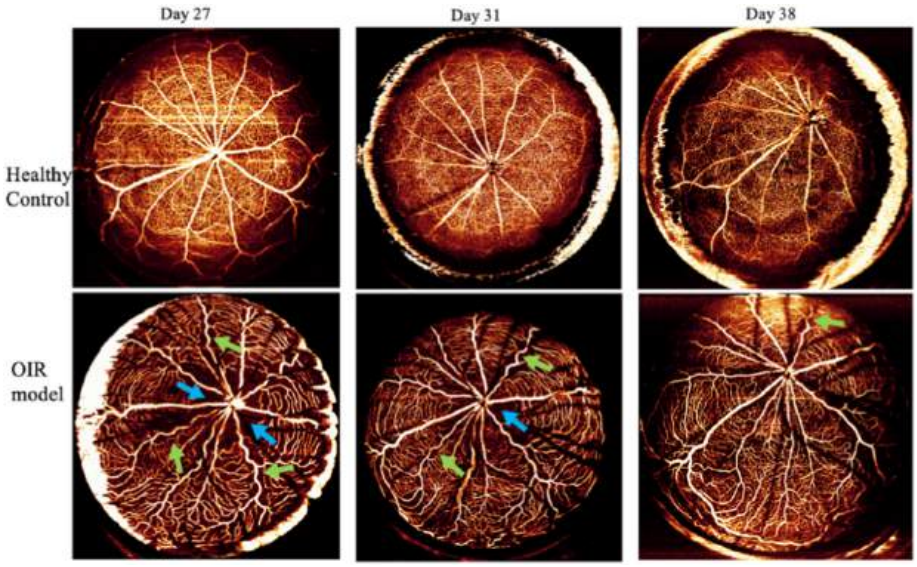

Fig. 9. High resolution 112° visual angle en face retinal OCTA images of a Brown Norway rat age-matched control and an oxygen-induced retinopathy rat taken by our custom designed ultra-wide field OCTA system at three different time points. Green arrows indicate torturous vessels; blue arrows indicate non-perfusion areas. Lower vessel density and increased tortuosity can be observed in the oxygen-induced retinopathy rat. With permission from (Liang et al., 2024). (For interpretation of the references to color in this figure legend, the reader is referred to the Web version of this article.)

a more sensitive indicator of image quality than the reflectance signal (Wei et al., 2019b). Therefore, image quality metrics that incorporate the flow signal can better guide operators to determine if a scan volume should be re-acquired even without the benefit of a visual cue.

Another way real-time processing can benefit OCTA is through motion tracking. As we noted above, most motion tracking in OCTA relies on allied imaging modalities, a scheme that has some important drawbacks. But if we can achieve real-time OCTA, we have the opportunity to

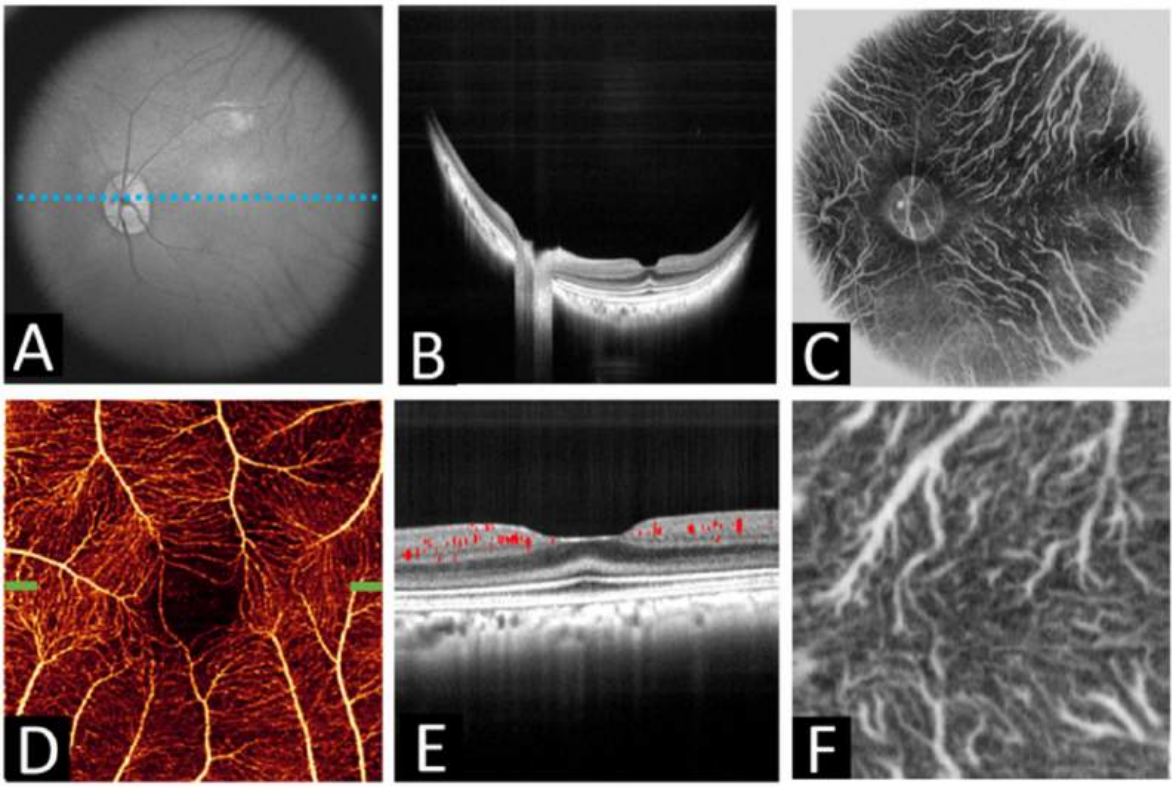

Fig. 10. A non-human primate with Batten disease and CLN7 mutation imaged with a lab-built device. Top row: full 60° visual angle field-of-view scan. (A) En face OCT image projected across the retina. (B) OCT B-scan image across the center field of view (at the location indicated by the dotted line in (A)), constructed by averaging over 5 B-scans. (C) En face projection from the choroid. Bottom row: a 3 × 3-mm scan of the same eye. (D) En face OCTA image of the inner retina. (E) Structural cross-section at the location of the green tick marks in (D) with retinal flow signal (red) overlaid, also constructed by averaging over 5 B-scans. Compared to a normal NHP the vessels in this animal do not form distinct plexuses. (F) 3 × 3-mm en face choroidal image in the structural channel. With permission from (Wei et al., 2024). (For interpretation of the references to color in this figure legend, the reader is referred to the Web version of this article.)

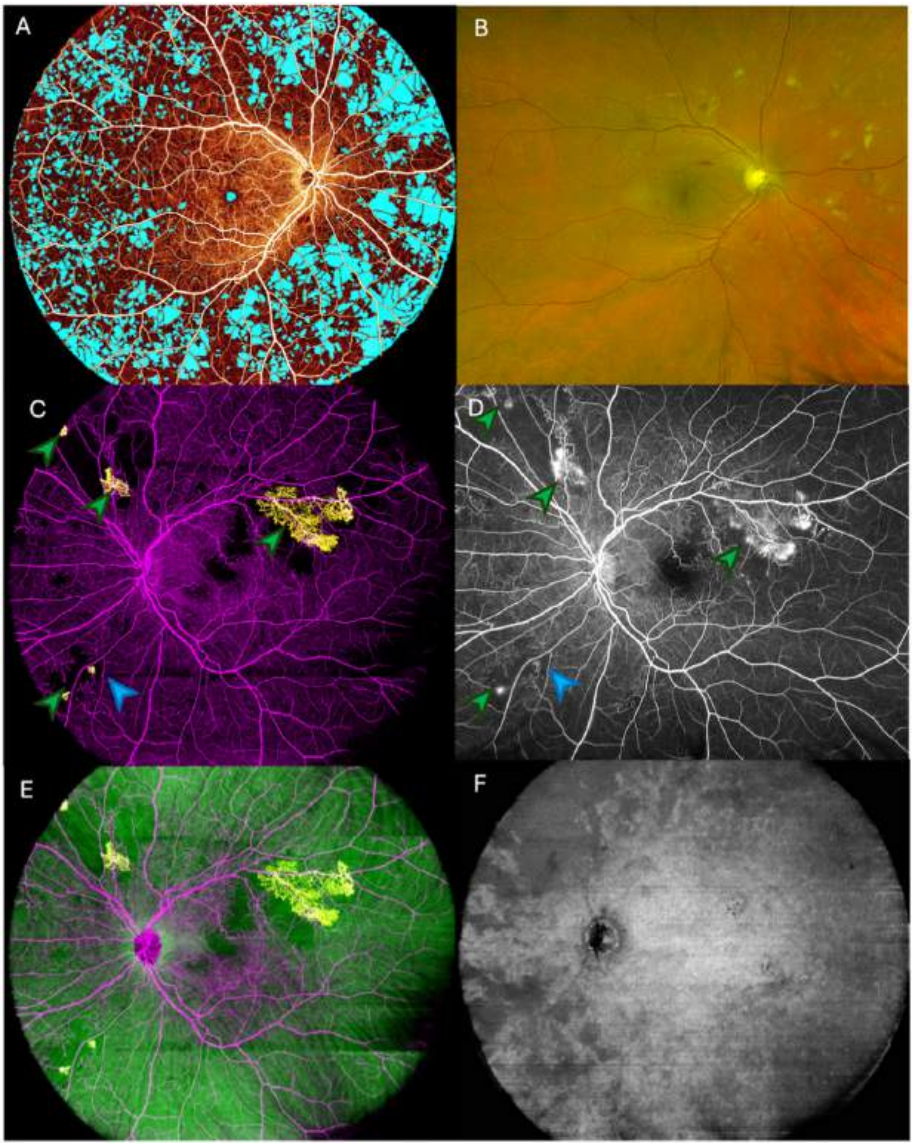

Fig. 11. 130-degree (eye angle) widefield OCTA images of eyes with DR compared to color fundus photography (CFP) and fluorescein angiography (FA). OCTA images were captured by a commercial device (DREAM Intalight). (A–B) An eye with non-proliferative DR. (A) Non-perfusion areas (teal) can be easily identified and quantified with OCTA. This task is substantially more difficult in CFP images (B). (C–F) An eye with proliferative DR. (C) OCTA can also easily identify retinal neovascularization (RNV; yellow) due to its location above the inner limiting membrane, which contrasts with retinal vasculature which is found below (purple). (D) The same eye imaged with fluoresceine angiography (FA). While RNV is also apparent in the FA image (green arrows in C and D), what appears to be an intraretinal microvascular abnormality (IRMA) is revealed to be RNV by OCTA (blue arrow). (E) A depth color-coded OCTA image enables assessment of vascular structure from above the ILM (yellow) through the retina (purple) and into the choroid (green). (F) This information could be correlated with a structural image of the ellipsoid zone, which shows photoreceptor loss in the mid-periphery. This damage would have been missed by conventional OCTA fields of view. (For interpretation of the references to color in this figure legend, the reader is referred to the Web version of this article.)

use the flow signal itself to provide tracking. In the self-navigation method (Wei et al., 2020) re-scanning is triggered when the ratio of the flow signal standard deviation to mean (an "instantaneous motion strength index") exceeds a threshold value. This quantity measures the amplitude of instantaneous motion by considering the number of cross-sectional scans that are unusually dark (caused by blink) or saturated (caused by microsaccade); these cross-sections can be easily noted in Fig. 6. This is just one metric that we could imagine using to identify the presence of artifacts using OCTA, but obviously any approach that relies on the flow signal will need to have it available in real-time.

3. Applications

3.1. Animal imaging

Model organisms are widely used in ophthalmology, both to investigate disease etiology/pathophysiology and to investigate new therapies. As with clinical imaging and research in humans, OCTA can be a powerful tool for imaging model organisms. In some cases system design may need to be modified due to different imaging requirements such as for smaller eyes.

An example is rodent imaging. Rodent models are among the most common across physiology, medicine, and biology due to short generation times, low cost, the availability of transgenic models, and genetic/anatomic similarity with humans. These models also benefit from a large

body of research across several disciplines. Rodent models are used in ophthalmology to study diabetic retinopathy (Robinson et al., 2012), glaucoma (Biswas and Wan, 2019; Di Pierdomenico et al., 2022; Morrison et al., 1997), retinopathy of prematurity (ROP) (Madan and Penn, 2003; Mezu-Ndubuisi et al., 2013; Smith et al., 1994), and rare retinal diseases (Vaquer et al., 2013). Among these, researchers can benefit from an extensive body of literature describing intraocular pressure (IOP) modulation and the fact that retinal vasculature develops postnatally (Fruttiger, 2002).

Human eyes, however, differ significantly from rodent eyes, particularly in size. To achieve superior imaging, it is beneficial to custom-design instruments tailored to their specific characteristics, which can be optimized using mathematical models of the rat and mouse eye (Hughes, 1979; Remtulla and Hallett, 1985). With such devices, OCTA images of rodent eyes can reveal vascular pathophysiology; for example, demonstrating modulation in blood flow due to ocular perfusion pressure can be monitored and measured (Pi et al., 2019, 2020; Zhi et al., 2012, 2015). Optical design issues become more acute when we attempt to capture widefield images of these eyes (Fig. 8) and can require modifications, such as an asymmetrical optical design (Liang et al., 2024). In this study, widefield imaging was able to show modulation of vascular pathology in an oxygen-induced retinopathy model (Fig. 9).

Another major difference between rodent eyes and human eyes is that rodents lack a macula. Given the importance of the macula to human vision this is a serious limitation in rodent models of ophthalmological diseases. If we want to study macular pathology in model organisms, we need non-human primate (NHP) models. Here a popular choice is the macaque. These models are important in particular for AMD (Gouras et al., 2008) and some inherited retinal dystrophies, where the similarity between human and macaque genomes means that there are macaque analogs to human diseases (Francis et al., 2008). These disease models, including a model for Batten disease (McBride et al., 2018), have been imaged with a widefield OCTA device designed for non-human primate imaging (Fig. 10) (Wei et al., 2024). Widefield-capable devices like these can allow researchers to examine how rare diseases develop in peripheral regions, improving our understanding of their etiologies and our ability to stage their progression.

3.2. Retinopathies

3.2.1. Diabetic retinopathy

Diabetic retinopathy (DR) is among the most prevalent vision-threatening vascular diseases and a leading cause of vision loss in working-age populations (Ting et al., 2016). Furthermore, its prevalence is growing (Guariguata et al., 2014), making it a major clinical priority. Non-proliferative DR (NPDR) changes include microaneurysms, intraretinal hemorrhages, foveal avascular zone (FAZ) enlargement, intraretinal microvascular abnormalities (IRMA), and capillary nonperfusion and hyperpermeability that result in retinal edema. Proliferative DR (PDR) is characterized by the presence of retinal neovascularization (Duh et al., 2017), which predisposes the eye for vitreous hemorrhage and traction retinal detachments.

Clinicians identify key features that predict increased risk of vision loss with clinical examination, color fundus photography (CFP), fluorescein angiography (FA), OCT, and, increasingly, OCTA. Relative to these allied modalities OCTA has several advantages. In head-to-head comparisons view several studies have shown that OCTA achieves better detection sensitivity than CFP for IRMA (Hwang et al., 2015; Schaal et al., 2019) and retinal neovascularization (RNV) (Russell et al., 2019a; Schwartz et al., 2020; Tsuboi et al., 2023; You et al., 2019) and detection sensitivity for non-perfusion area (NPA) that is comparable (Sawada et al., 2018) or better than FA (Couturier et al., 2019; Decker et al., 2023; Hwang et al., 2016, 2018; Silva et al., 2015). Importantly, OCTA can also localize features in 3-dimensions due to simultaneous and co-registered structural OCT acquisition. Unlike 2-dimensional modalities like the FA, this allows objective detection of RNV based on its anatomic location (Ito et al., 2020), differentiation of RNV from IRMA, characterization of vitreous attachment to RNV, evaluation of non-perfusion in different retinal vascular plexuses (Hwang et al., 2018), localization and characterization of microaneurysms in 3-dimensions (Gao et al., 2024; Schreur et al., 2019), and assessment of their perfusion status (Gao et al., 2022b, 2024).

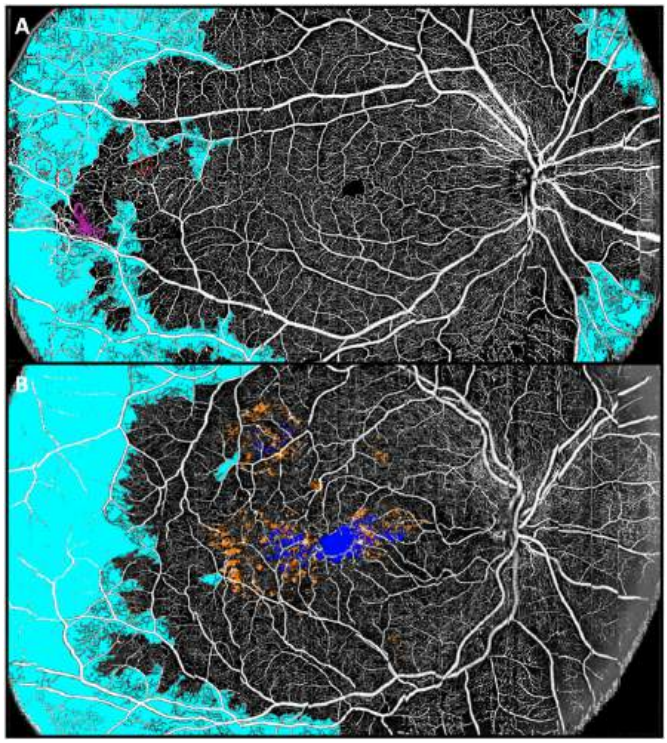

Fig. 12. Widefield imaging (75° visual angle) of multiple pathologic features in eyes with diabetic retinopathy (DR) using a lab-built device. (A) A 12 × 23-mm en face image of the inner retina of an eye with proliferative DR shows extensive non-perfusion areas (teal), retinal neovascularization (purple; identified by its location anterior to the inner limiting membrane), and microaneurysms (red, circled) in the temporal periphery. (B) An eye with diabetic macular edema captured within the same field of view also reveals an extensive non-perfusion area (teal). By combining with the structural image, lipid extravasation, which manifests as hyperreflective foci (orange), and retinal fluid (blue) can be imaged simultaneously. These 12 × 23-mm images were captured with 10 μm/pixel transverse sampling density. (For interpretation of the references to color in this figure legend, the reader is referred to the Web version of this article.)

With first generation OCTA, all of these advantages had to be weighed against small fields of view. With current instruments this is no longer the case, and visual comparison indicates some advantages for OCTA (Fig. 11). These wider fields of view are overcoming some of the main clinical limitations of standard field OCTA. For example, RNV is primarily found outside the macula and especially around the disc and the major arcades (Russell et al., 2019a). OCTA that covers these areas at a minimum is essential to be clinically useful for detection of RNV (Russell et al., 2019b; Sawada et al., 2018). For RNV lesions within view, studies have indicated that OCTA outperforms FA in RNV detection (Pichi et al., 2020; Stino et al., 2024) and can detect RNV that was overlooked with CFP in clinical examinations (Tsuboi et al., 2023). Because OCTA can be obtained quickly without the need for dye injection, it could potentially be used for routine surveillance of RNV and treatment response (Cui et al., 2021; Li et al., 2022; Russell et al., 2020, 2022). A wider field of view is also advantageous for NPA detection. NPA may be found mostly outside the macular region (Fan et al., 2017; Silva et al., 2015) (Fig. 12). A wider field of view is also important for diagnosis. Despite achieving higher detection sensitivity for NPA, in one

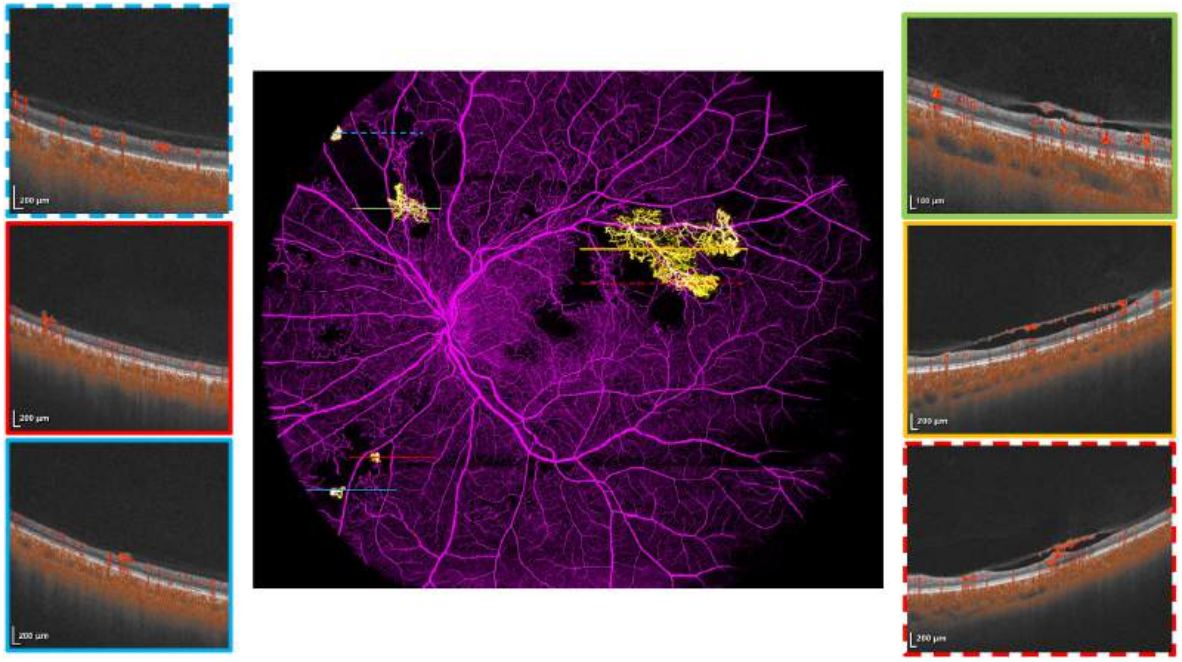

Fig. 13. Retinal neovascularization (RNV) with and without posterior vitreous detachment (PVD) visualized with OCTA. The neovascular vessels are shown in yellow in the widefield image and can be readily separated from the retinal circulation (violet) due to their location above the inner limiting membrane. Cross-sectional images show the RNV profiles at the various scan locations indicated. The cross-sections on the left show examples of RNV without PVD while the cross-sections on the right show cases with partial PVD with RNV forming along the outer surface of the posterior hyaloid face. These images were captured with a 130° eye angle commercial device (DREAM, Intalight). (For interpretation of the references to color in this figure legend, the reader is referred to the Web version of this article.)

study OCTA with a conventional field of view was less accurate for staging DR than widefield dye angiography (Decker et al., 2023). This disadvantage was reversed with a comparable field of view in the same study. In addition, one can always quantify RNV and NPA with OCTA as the vascular pathology is not confounded by leakage or laser scars in the deeper layers (Guo et al., 2021). While there are specific artifacts in OCTA that can also confound quantification (De Pretto et al., 2019), these can be addressed with deep learning-based approaches (Guo et al., 2019). All of these capabilities can lead to a more objective and rational approach to clinical management of diabetic retinopathy (Fig. 13).

The 3-dimensional aspect of widefield OCTA, combined with automated detection and quantification of features, allows for the testing of more hypotheses *in vivo*. Examples include a widefield OCTA study finding RNV associated with ischemia (Shiraki et al., 2022; Stino et al., 2023). OCTA can also identify preclinical pathology, and longitudinal studies have indicated how features like IRMA (Russell et al., 2020) or RNV sprouts (Tsuboi et al., 2024) can develop into RNV. Furthermore, the relationship between retinal neovascularization (RNV) and posterior vitreous detachment (PVD) in proliferative diabetic retinopathy (PDR) is intrinsically tied to the vitreoretinal interface. The posterior hyaloid face often acts as a scaffold for the growth of RNV, while partial or incomplete PVD, frequently associated with vitreoschisis, creates structural conditions conducive to neovascular proliferation and anchoring to the vitreous cortex (Russell et al., 2021; Vaz-Pereira et al., 2017). Widefield OCTA can provide powerful analysis such as this to RNV lesions throughout the retina, an important capability since the pathology can be found from the posterior pole to the periphery (Fig. 12).

3.2.2. *Retinal vein occlusions*

Retinal vein occlusions (RVO) are the most common ocular vascular disorder after DR (Song et al., 2019) and can lead to severe vision loss (Pulido et al., 2016). A blockage of the central retinal vein or a major branch causes congestion within the capillaries leading to nonperfusion and edema. Related nonperfusion, retinal edema, and secondary neovascularization can cause vision loss (Jaulim et al., 2013). CFP can detect many implicated features (Parodi and Bandello, 2009), while specific features such as perfusion loss and edema are conventionally and more clearly imaged with dye angiography (Prasad et al., 2010) and structural OCT (Spaide et al., 2003), respectively.

Widefield OCTA can be useful in the evaluation of nonperfusion and detection of RNV. Vascular pathology related to BRVO can be imaged by OCTA as well as FA (Figs. 14 and 15). Conventional (Nobre Cardoso et al., 2016; Seknazi et al., 2018) and widefield OCTA (Glacet-Bernard et al., 2021; Kadomoto et al., 2021; Shiraki et al., 2019) measurements of non-perfusion both correlate with FA. However, widefield OCTA may be better suited for detection of neovascularization (Huemer et al., 2021), the timely detection and treatment of which has been demonstrated to reduce risk of vision loss (Branch Vein Occlusion Study Group, 1986). The extent of NPA, also better viewed on widefield, can further indicate the risk of neovascularization, and furthermore provides prognostic information for vision on its own (Seknazi et al., 2018). A widefield OCTA study also found that collateral vessels are most often found outside the macula(Rudnik et al., 2023), which provides another clinically relevant reason for expanding the OCTA field of view.

3.2.3. *Retinopathy of prematurity*

Retinopathy of prematurity (ROP) is a leading cause of childhood blindness and can occur when preterm infants receive supplemental oxygen that, while lifesaving, can cause delayed development and aberrant vascularization of the retina (Hellström et al., 2013; SUPPORT Study Group of the Eunice Kennedy Shriver NICHD Neonatal Research Network, 2010). Ophthalmoscopy can be used for screening the disease (Fierson, 2018), but given its vascular nature OCTA is an attractive alternative. That is, provided the technique can be adapted for neonate imaging. The technical hurdles to overcome are the inability to use fixation targets and a limited timeframe for imaging due to uncooperative patients that typically begin to cry during procedures. Handheld OCT devices are a means of dealing with these challenges (Yang et al.,

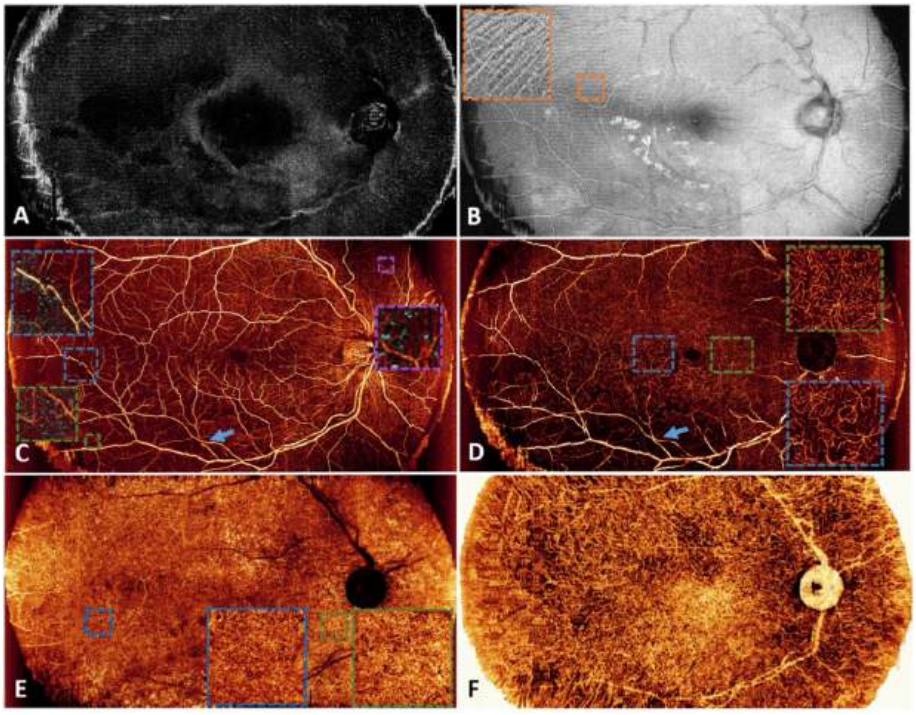

Fig. 14. High-resolution, widefield imaging of an eye with branch retinal vein occlusion. Throughout, color coded dotted boxes show magnifications of notable features. (A) A 12 × 23-mm structural image of the region extending from the inner limiting membrane 10 μm into the vitreous. Macrophage-like cells can be identified as bright white dots. (B) Nerve fiber layer structural image. The magnification shows individual nerve fibers. (C) Superficial vascular complex angiogram. Here, the structural image showing macrophage-like cells is overlaid in teal. In the purple box, which is in an area unaffected by the vein occlusion, macrophage-like cells appear evenly distributed, with no obvious correlation to the underlying vasculature. The same is true in a magnification of non-perfused area downstream of the occlusion (green box). However, in other locations the macrophage-like cells appear to cluster around vessels adjacent to non-perfusion areas (blue box). (D) Deep vascular complex angiogram. The non-perfused area appears larger in the deep vascular complex image (blue arrows in (C) and (D) at the same location for comparison). (E) Choriocapillaris angiogram. Magnifications of the regions in the blue and green boxes show similar intercapillary spacing in both the region of the eye afflicted by the vein occlusion (blue box) and in a region with healthy perfusion in the more superficial layers (green box). (F) In Sattler's layer it is also difficult to observe clear pathology in the region of the occlusion. These 12 × 23-mm image was captured with 10 μm/pixel transverse sampling density. (For interpretation of the references to color in this figure legend, the reader is referred to the Web version of this article.)

2017a).

In ROP, handheld OCTA can be used to differentiate types of neovascularization (Chen et al., 2024) and monitor the effect of therapeutic interventions (Campbell et al., 2017a). While these studies were able to detect vascular pathology using OCTA, structural OCT measurements indicate that many pathologic features in ROP are peripheral (Nguyen et al., 2022). Handheld widefield OCTA can also assess vascular pathology OCTA (Fig. 16) (Campbell et al., 2017b; Ni et al., 2021, 2024). ROP is a lifelong disease, and older children and adults with ROP can be imaged using commercial devices. In a case imaged using an Intalight DREAM OCT device, abnormal vessels are notable in the far periphery (Fig. 17).

3.2.4. *Sickle cell retinopathy*

Sickle cell retinopathy (SCR) is a vision-threatening complication of sickle cell disease characterized by peripheral arteriolar occlusion, capillary nonperfusion, and neovascularization (Goldberg, 1971). A meta-analysis revealed that patients with SCR exhibited a significantly enlarged foveal avascular zone and reduced vessel density in both the superficial and deep capillary plexus compared to healthy controls (Clarke et al., 2025). These findings highlight the ability of OCTA to quantitatively assess microvascular pathology, providing objective evidence of retinal vascular changes in SCR. Additionally, the non-perfusion ratio measured on widefield OCTA provides diagnostic information regarding SCR severity and may serve as a predictive marker for disease progression (Fig. 18) (Bistour et al., 2023). A significant reduction in capillary density, particularly in the temporal macular region of proliferative SCR patients, has been correlated with visual field scotomas (Jung et al., 2018), highlighting the utility of widefield OCTA in visualizing layered vasculature and its potential functional relevance.

3.2.5. *Coats disease and Coats plus syndrome*

Coats disease is a rare, idiopathic retinal vascular disorder characterized by retinal telangiectasia, aneurysmal dilatation, and subretinal exudation (Shields et al., 2001). It predominantly affects young males and typically presents unilaterally. In contrast, Coats plus syndrome is cerebroretinal microangiopathy caused by CTC1 mutations, featuring bilateral retinal telangiectasia along with neurologic and visceral abnormalities, such as cerebral calcifications, leukodystrophy, and gastrointestinal bleeding (Chaaya et al., 2025). Given that the pathology in both Coats disease and Coats plus syndrome often involves the peripheral retina, widefield OCTA provides significant advantages in assessing peripheral microvascular alterations, including telangiectasia, ischemia, and vascular remodeling (Fig. 19). Its noninvasive and repeatable characteristics make it particularly valuable for longitudinal monitoring in pediatric patients (Ponugoti et al., 2022).

3.2.6. *Inherited retinal dystrophies*

Inherited retinal diseases (IRD) are a diverse group of genetic diseases that can present throughout life and may lead to blindness (Henderson, 2019). Because they are rare, they can be difficult to study. They may have overlapped and variable clinical phenotypes, and the precise diagnosis can require extensive testing. Widefield OCTA can potentially improve both the diagnosis and monitoring of these conditions. We give some examples below.

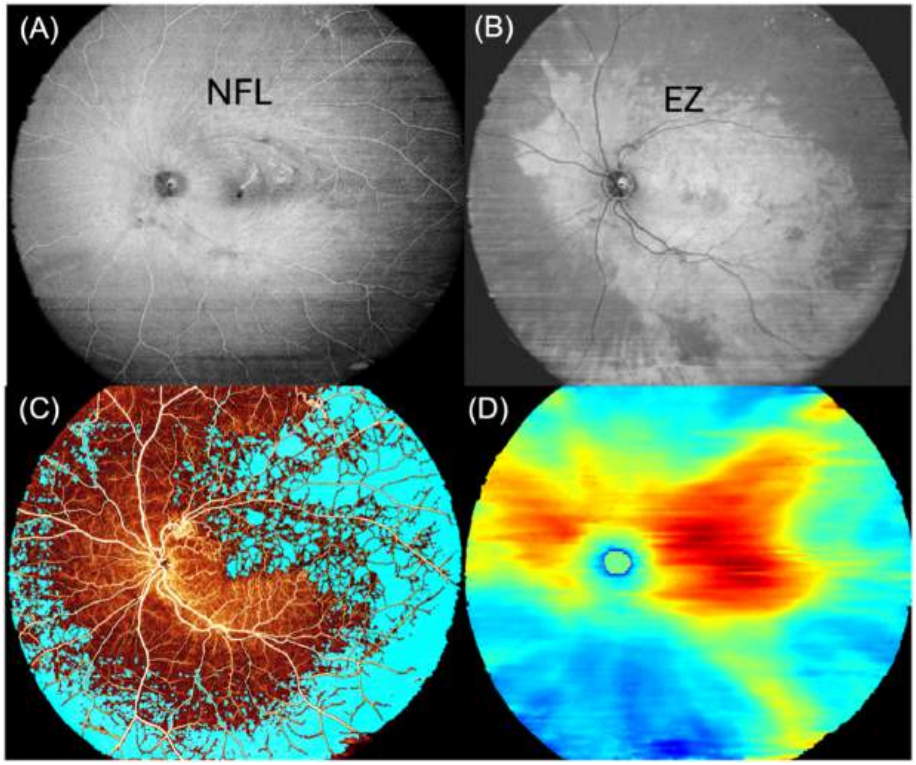

Fig. 15. A BRVO case imaged with a commercial widefield system (Intalight DREAM OCT). In this case the NFL (A) appears relatively intact while the ellipsoid zone loss (B) and non-perfusion area (C) appear to coincide. Retinal thinning (D) also appears to be most extensive in the quadrant most affected by perfusion and ellipsoid zone loss.

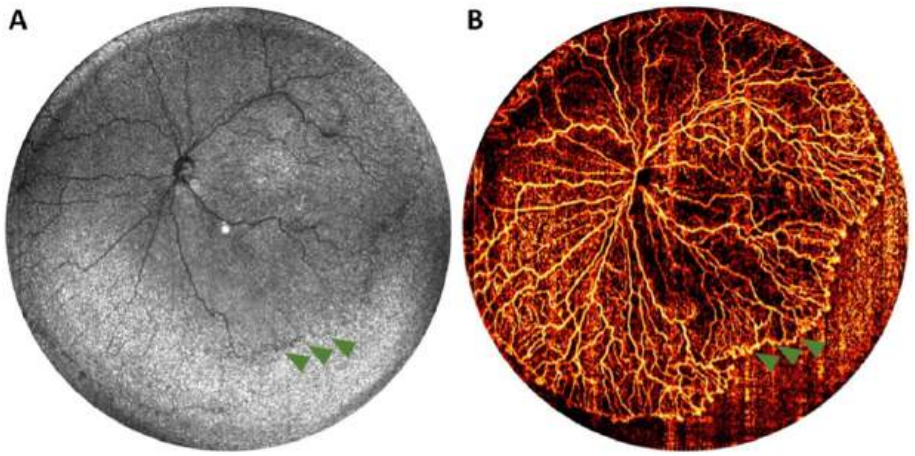

Fig. 16. Panretinal imaging in retinopathy of prematurity (ROP) using a handheld device. (A) En face OCT image of the right eye from an infant (born at 23 weeks gestation, 593 g, and imaged at 38 weeks postmenstrual age) with ROP stage 1, where the fibrovascular ridge is marked by green arrowheads but is not distinctly visible in the structural en face image. (B) The corresponding en face OCTA heatmap, which enhances the visualization of the vascularized retina, providing greater clarity and detail. (For interpretation of the references to color in this figure legend, the reader is referred to the Web version of this article.)

Choroideremia. Choroideremia is a recessive, X-linked retinal dystrophy that leads to nyctalopia, visual field restriction, and blindness (Flynn Roberts et al., 2002). Pathoanatomic changes induced by the disease include degeneration of the choriocapillaris, retinal pigment epithelium (RPE), and photoreceptors (Rodrigues et al., 1984). Previous OCTA reports have registered these changes in conjunction with structural OCT, noting that regions of RPE, photoreceptor, and choriocapillaris loss tend to overlap. (Carlyle et al., 2015; Gao et al., 2017; Jain et al., 2016). Retinal perfusion loss also tends to be concentrated in the deep capillary plexus (Gao et al., 2017). In widefield images, it is clear that the macula tends to be spared (Fig. 20).

Retinitis Pigmentosa is among the most common IRD (Hartong et al., 2006). Disease progression is typically monitored by electroretinogram (Grover et al., 2003), visual field (Holopigian et al., 1996), and structural OCT (Hariri et al., 2016). Like choroideremia, conventional OCTA demonstrates that in retinitis pigmentosa most perfusion loss occurs in the deep capillary plexus (Hagag et al., 2019; Koyanagi et al., 2018; Parodi et al., 2017; Takagi et al., 2018). By comparison with structural OCT and visual field we can determine that these pathologic vascular changes correlate with retinal thinning (Hagag et al., 2019; Toto et al., 2016) and visual function (Murakami et al., 2014; Toto et al., 2016). With widefield OCTA, it is additionally apparent that mid-peripheral

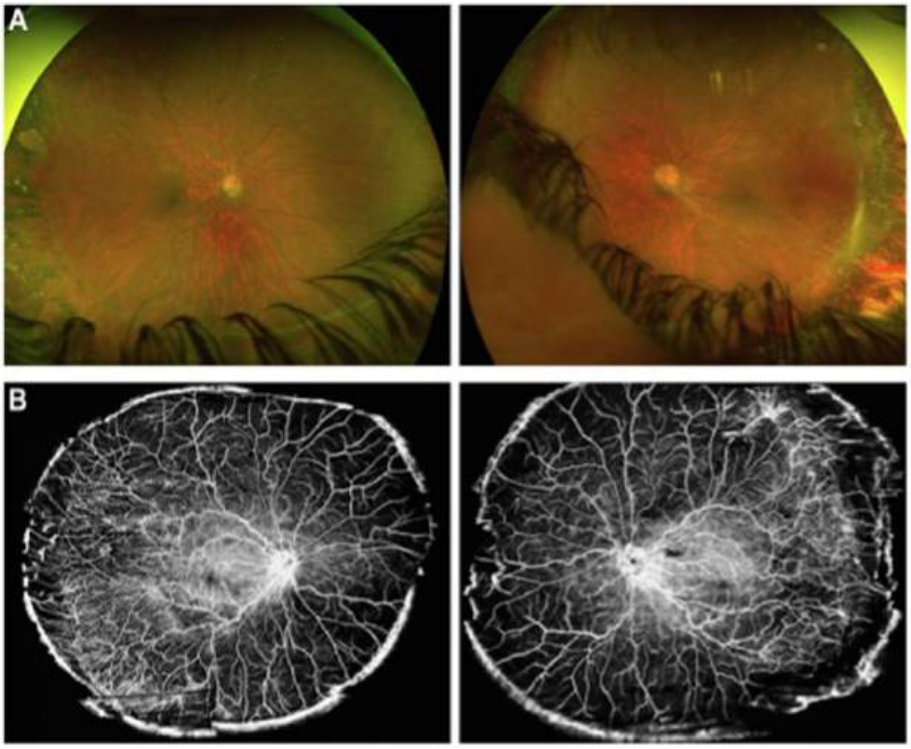

Fig. 17. A 26-year-old man was referred for retinopathy of prematurity with history of laser treatment and cryotherapy. Fundus examination (**A**) showed disc dragging, vessel tortuosity, and peripheral regressed ridges with retinal scars and fibrous proliferation in both eyes. The ultra-widefield swept-source OCT angiography montage (**B,** DREAM OCT, Intalight) reveals dilated and torturous peripheral blood vessels with abnormal branching, stretched and straightened vessels, as well as possible arteriolar-venular shunt near the ridge in the temporal periphery of both eyes, highlighting persistent vascular alterations from prematurity. Advancements in ultra-widefield swept-source OCT angiography enable rapid, noninvasive, peripheral vascular imaging, facilitating monitoring of retinopathy of prematurity patients.

regions are more strongly affected by perfusion loss than the posterior pole (Mastropasqua et al., 2020) (Fig. 21).

3.3. Uveitis

Uveitis is an encompassing term for a diverse group of vision-threatening diseases that cause inflammation of the uvea (iris, ciliary body, and choroid) and often surrounding tissue including the retina (de Smet et al., 2011). In part because of the diversity of these diseases, and in part because they are difficult to classify, estimates of the prevalence of uveitis are imprecise, ranging from 38 to 714 cases per 100,000 (García-Aparicio et al., 2021); uveitis could account for as much as 10 % of visual impairment in the world (Miserocchi et al., 2013). It can be classified both anatomically (anterior, intermediate, posterior, pan-uveitis) and etiologically (infectious, non-infectious), with non-communicable forms being more prevalent (Huang and Brown, 2022). Clinical management of uveitis relies on correct diagnosis of both these anatomical and etiological classifications (Guly and Forrester, 2010).

Conventional OCTA has demonstrated utility in uveitis for detecting and differentiating choroidal neovascularization (CNV) from inflammatory lesions and monitoring CNV response to anti-VEGF therapy (Cheng et al., 2016; Levison et al., 2017; Tang et al., 2020; Zahid et al., 2017), visualizing and quantifying microvascular abnormalities and perfusion loss in the retinal plexuses (Aggarwal et al., 2018; Kim et al., 2016), and flow deficits in the choriocapillaris (Klufas et al., 2017).

Extending these capabilities to the periphery improves OCTA characterization of uveitis. Allied imaging modalities like dye angiography can also accomplish peripheral imaging, but OCTA is unique in its ability to anatomically isolate vascular tissue. For example, one report found that in intermediate uveitis, specific (deeper) layers of vascular tissue may display more pathology (Tian et al., 2019) (Fig. 22). This is a result that would be impossible to replicate with dye angiography. Widefield OCTA imaging has also been applied to specific non-infectious uveitides. Behcet's disease is an autoinflammatory disease caused by Th1 and Th17 cell dysregulation (Yang et al., 2021). A widefield OCTA study found that the peripheral and parafoveal deep capillary plexus was most affected by the disease and that measurements of flow area in this tissue could be used for sensitive diagnosis. These measurements also correlated with visual acuity (Dai et al., 2024). Vogt-Koyanagi-Harada is another autoimmune uveitis prevalent in China (Yang et al., 2005). With widefield OCTA, vessel dilations along with flow voids are visible when the disease is active while persistent flow index loss in the choriocapillaris can be seen when the disease is inactive. Reduced flow in the inactive state could be used to assess disease activity in this study (Qian et al., 2021). Widefield OCTA can also assess idiopathic uveitis. A good example is a widefield OCTA imaging of Eales disease (Nakamura et al., 2024) (Fig. 23), a vasculopathy characterized by ischemia progressing to neovascularization and recurrent hemorrhage (Biswas et al., 2002). In this case extensive perfusion loss, extensive neovascularization, and arteriovenous shunts are apparent but confined to the periphery. In a case study, Nakamura et al. reported that OCTA improved visualization of laser photocoagulation treatment response (Nakamura et al., 2024).

3.4. Ocular oncology

Widefield OCTA is a useful technology for oncology since tumors can appear throughout the retina. We give two examples of the application of widefield OCTA to oncology.

von Hippel-Lindau disease is characterized by multifocal tumors (Conway et al., 2001), including hemangioblastomas of the retina, which are frequently the first presentation of the condition (Varshney

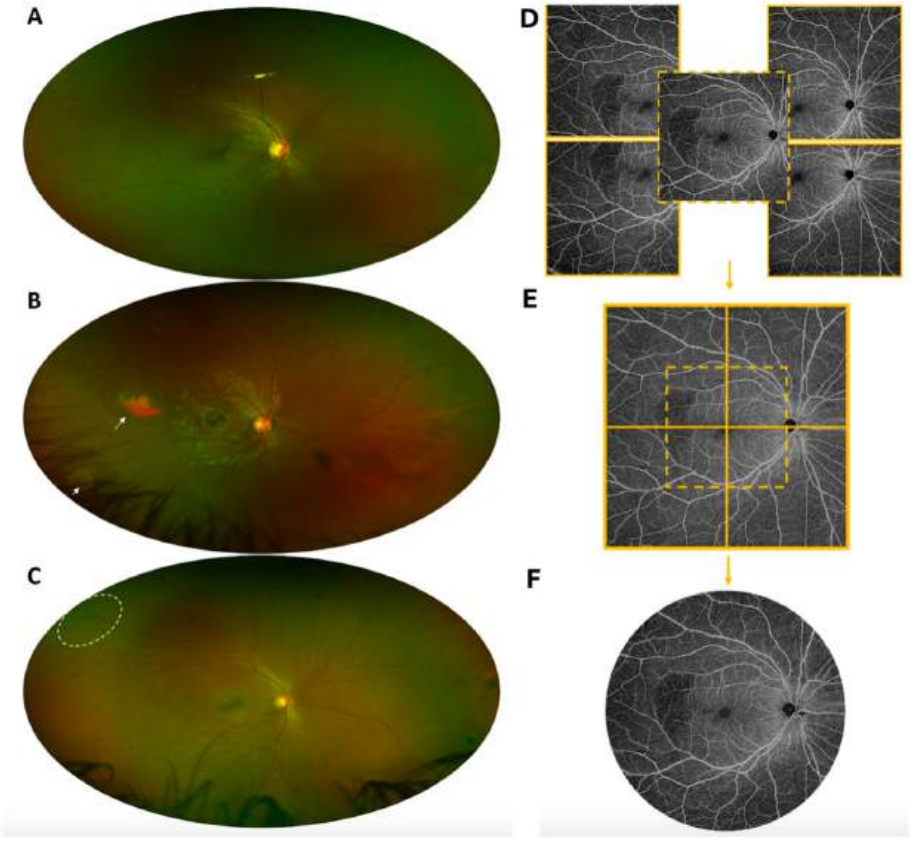

Fig. 18. Representative widefield imaging in sickle cell retinopathy (SCR). (A–C) Ultra-widefield color fundus photographs (Optos) demonstrate SCR stages: (A) no retinopathy; (B) non-proliferative SCR with a salmon patch hemorrhage (large arrow) and peripheral black sunburst (small arrow); (C) proliferative SCR with peripheral neovascularization (circle). (D–F) Widefield en face OCTA image: (D) five individual 12 × 12-mm scans, (E) merged into montage widefield scan, and (F) automated reconstruction of the widefield en face OCTA covering an approximately 21 × 21-mm field of view. (For interpretation of the references to color in this figure legend, the reader is referred to the Web version of this article.)

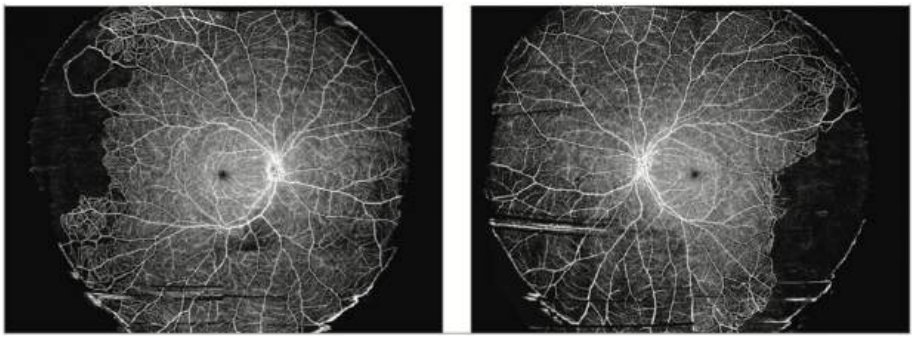

Fig. 19. Widefield en face OCTA in Coats plus syndrome shows peripheral telangiectatic vessels, intercapillary dropout, and vascular shunting in bilateral eyes.

et al., 2017). A majority of individuals affected by the disease demonstrate retinal capillary hemangioblastomas, of which the majority are peripheral rather than central (Wong et al., 2008). This makes screening using widefield OCTA a useful strategy for the disease. In one study, ophthalmoscopy missed 71.4 % of retinal hemangioblastomas detected using widefield OCTA, indicating that OCTA is effective for early detection of small and mid-peripheral tumors (Lang et al., 2024) (Fig. 24).

Choroidal melanoma is the most common primary intra-ocular neoplasm, second most common malignant melanoma site (Soliman et al., 2023). Clinically, the most challenging aspect of the disease is distinguishing small melanomas from benign nevis. This task is well suited to OCTA, which differentiates between nevi subtypes (flat and elevated) (Greig et al., 2021). Another application for OCTA is monitoring treatment response (Lim et al., 2020) (Fig. 25).

4. Future work

Widefield OCTA is becoming increasingly accessible for clinical practice and research, but the technology remains in its early stages, leaving ample room for improvement through ongoing technical innovation.

Some important widefield OCTA system components should not be considered optimized. Advanced technologies like VCSEL illumination, which offer a more reliable alternative to FDML devices (Ni et al., 2021; Zhang et al., 2021), are not yet widely available. The larger imaging

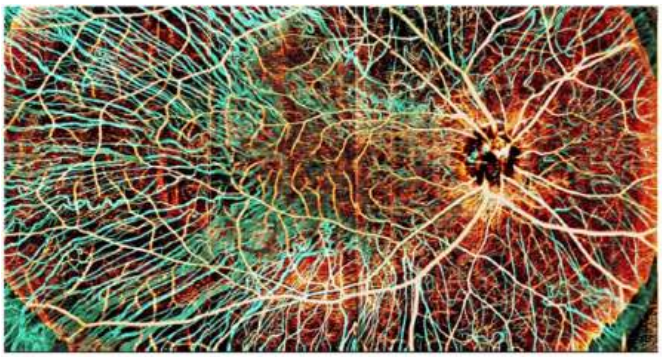

Fig. 20. An eye with choroideremia imaged with a lab-built widefield (75° visual angle) OCTA device. In this image, vessels are color coded according to depth with retinal vessels in sepia and choroidal vasculature in teal. In the macular region, the preserved retinal pigment epithelium and photoreceptors block imaging of the large choroidal vessels. Loss of these structures are mostly apparent in the peripheral regions. (For interpretation of the references to color in this figure legend, the reader is referred to the Web version of this article.)

areas in widefield OCTA necessitate lower illumination to comply with ANSI protocols which translates into less signal at the detector. Incorporating more efficient detection methods, such as avalanche photodiodes or balanced detection systems (Choma et al., 2003), into next-generation devices could help mitigate this signal reduction and enhance overall performance.

System improvements can improve the number and types of pathologies that can be detected with OCTA. But one of the biggest advantages OCTA can provide is the ability to quantify these features in order to improve clinical inference and better evaluate therapeutic efficacy. State-of-the-art quantification techniques in OCTA rely on AI (Hormel et al., 2021c; Schmidt-Erfurth et al., 2018). There are many examples of these tools working at the human level or superhuman level on research data sets with conventional fields of view: success in tasks including segmenting macular neovascularization (Wang et al., 2023a) and NPA (Guo et al., 2019), image quality assessment (Lauermann et al., 2019) and enhancement (Abu-Qamar et al., 2023; Gao et al., 2020, 2021), and disease diagnosis (Lee et al., 2023; Zang et al., 2022, 2023) have all been demonstrated. Tasks including artery/vein differentiation (Abtahi et al., 2022) or identification of projection artifacts (Wang et al., 2022) that are difficult for humans can also be amenable to AI (semi)-automation. But extending these capabilities to the periphery is not a trivial task. AI relies on large data sets for training. As larger datasets become available these methods will become more powerful, but the size of the datasets involved can become prohibitive. Training AI is computationally intensive, and using large images increases costs substantially. A practical solution is to train on smaller image sub-regions, which helps manage computational costs while still achieving effective widefield results (Gao et al., 2022a; Guo et al., 2021).

One of the key advantages of OCTA over other vascular imaging modalities is its ability to provide volumetric imaging, particularly for chorioretinal anatomy, enabling the isolation of individual plexuses. Since OCTA data are primarily analyzed using *en face* orientations that rely on projections across segmented anatomic layers, accurate plexus segmentation is essential. While plexus definitions are well-established for posterior pole imaging, the peripheral vascular anatomy remains less defined, with plexus definitions in the periphery still awaiting standardization. In the periphery, plexuses that maintain a laminar orientation near the fovea become increasingly intertwined (Campbell et al., 2017c). We require both clinically meaningful plexus definitions in the periphery, and the technical means to implement their visualization.

Another area to improve is system cost. Key components in widefield OCTA systems, particularly swept-source illumination, remain prohibitively expensive for many applications. Additionally, as previously mentioned, AI training is significantly more computationally intensive for widefield OCTA compared to conventional fields of view, making

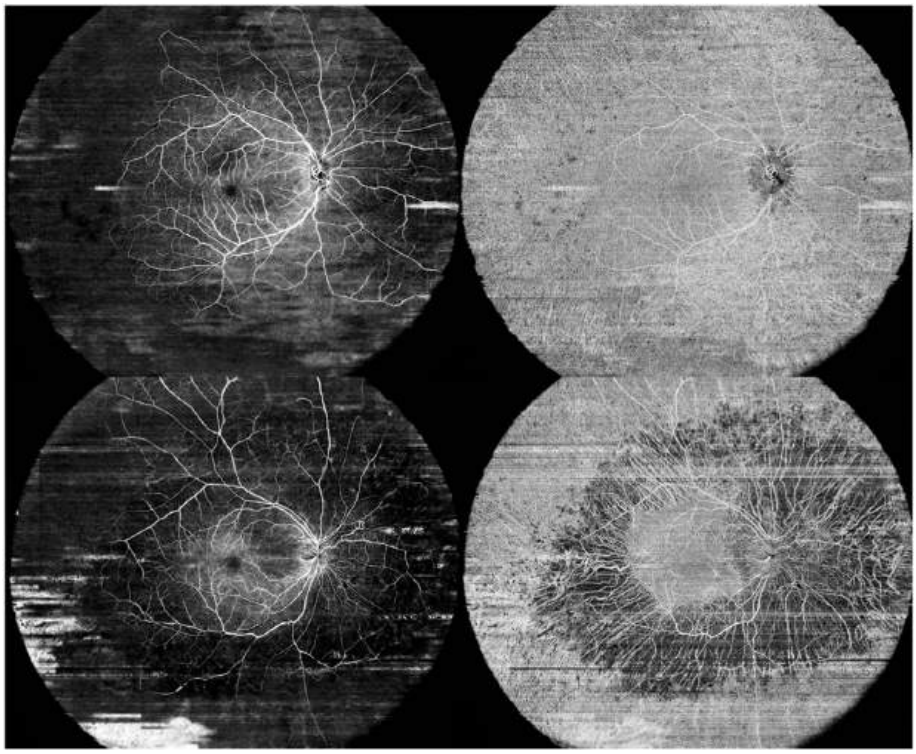

Fig. 21. *130-degree (eye angle) OCTA images of retinitis pigmentosa. Device output from a widefield OCTA device (DREAM Intalight) showing different degree of perfusion loss in the inner retina (left) and choriocapillaris (right). Row 1: An eye with retinitis pigmentosa showing perfusion loss confined to the peripheral retina. Row 2: An eye with a more advanced defect, revealing areas with large choroidal vessels exposed. Some segmentation and motion artifacts are apparent in the device output.*

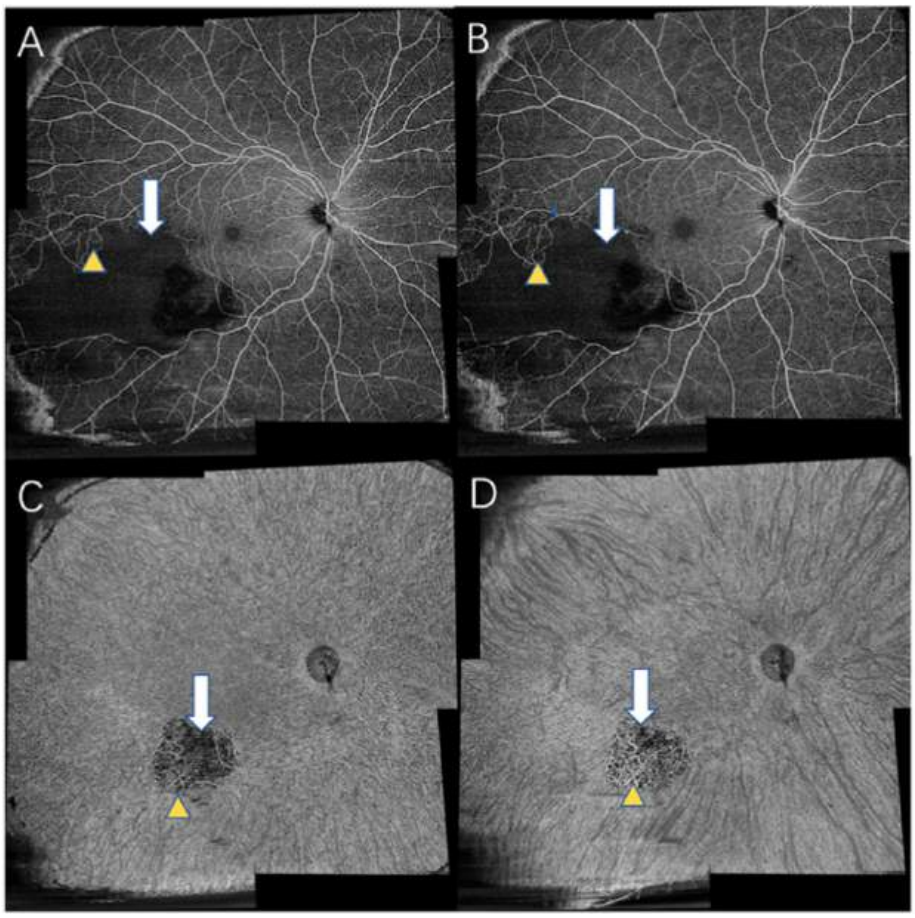

Fig. 22. Non-perfusion (white arrow) and reduced perfusion (yellow triangle) in an eye with intermediate uveitis. (A) superficial vascular complex, (B) deep vascular complex, (C) choriocapillaris, and (D) choroid imaged with a Zeiss PLEX elite 9000. With permission from (Tian et al., 2019). (For interpretation of the references to color in this figure legend, the reader is referred to the Web version of this article.)

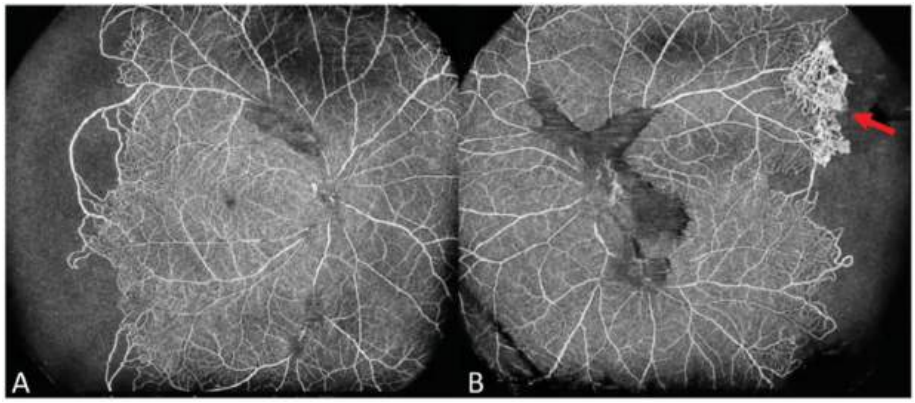

Fig. 23. Widefield OCTA of an eye with Eale's disease. Widefield OCTA revealed an extensive nonperfusion area in the peripheral fundus of the right eye (A) and left eye (B) and prominent retinal neovascularization in the superior temporal area (red arrow) in the left eye (B). The image is at the level of the superficial retinal layer and includes the area on the vitreous side that starts at 10 μm from the inner limiting membrane and continues to the border between the inner plexiform layer and the inner nuclear layer. These images were captured using a Xephilio OCT- S1 (Canon). With permission from (Nakamura et al., 2024). (For interpretation of the references to color in this figure legend, the reader is referred to the Web version of this article.)

hardware costs for image processing a considerable concern. While GPUs are essential for widefield OCTA, their development is driven primarily by other industries, such as cryptocurrency mining and large language models, rather than medical imaging. On a positive note, researchers in widefield OCTA are continuously advancing swept-source technology to improve accessibility and reduce costs.

The hope for widefield OCTA is that it will ultimately prove a clinically relevant technology. System cost is an important bottleneck for introducing new devices into the clinic. Another requirement is that the technology has a demonstrated use-case in a clinical environment. We think that it is likely that that this is true: conventional OCTA has demonstrated the ability to stage diagnose and stage disease (Hormel et al., 2021c; Spaide et al., 2018). While these are not unique capabilities for OCTA there are tasks for which it is particularly well-suited. These

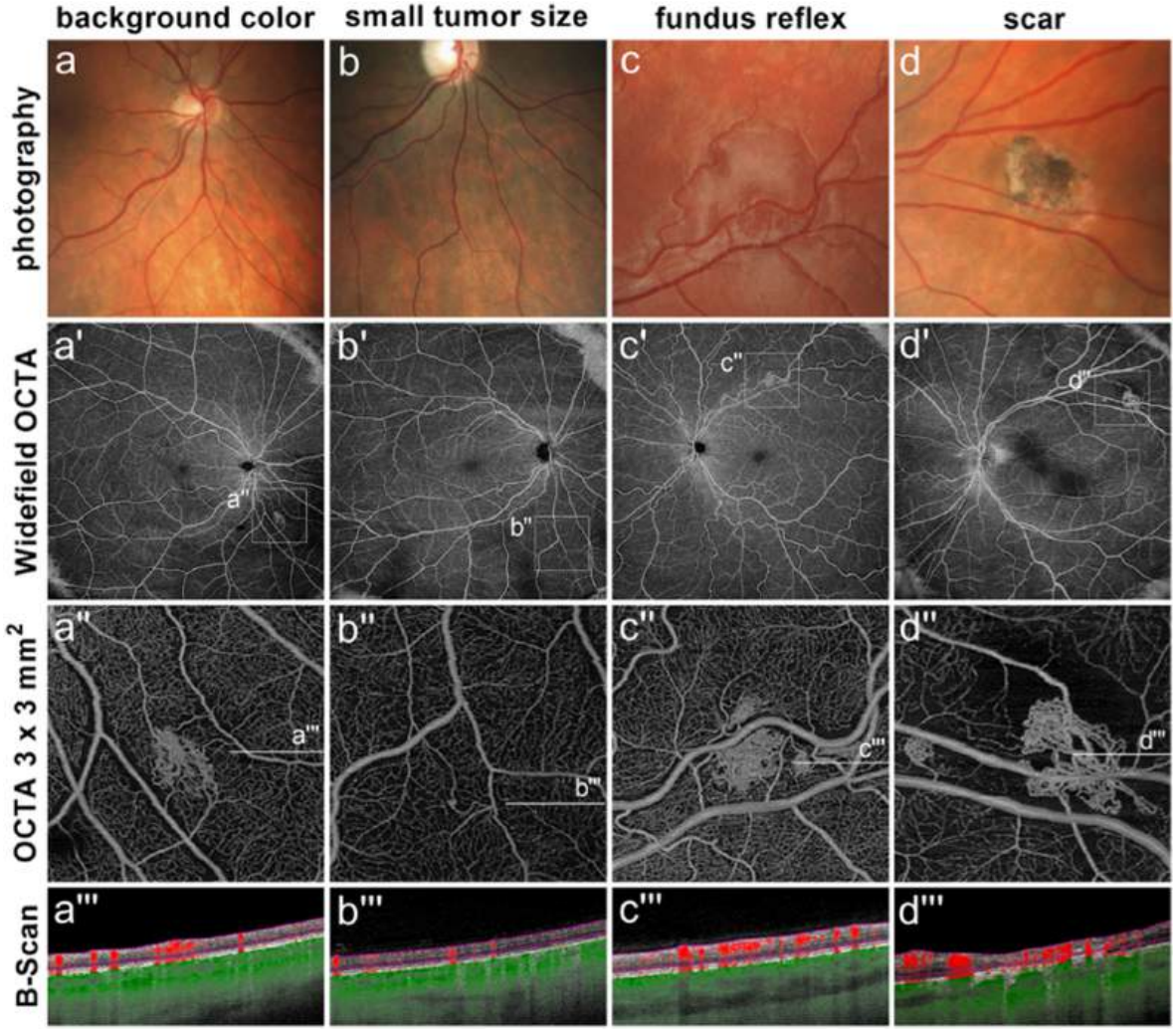

Fig. 24. An eye with von Hippel Landau syndrome. Retinal hemangioblastomas overlooked by photography (a–d), detected using widefield OCTA from a Zeiss PLEX elite 9000 (a'-d'), zoom-ins to the regions indicated in a'-d' (a"-d"), and cross-sections with OCTA overlay (red: retinal flow; green: choroidal flow). In (a) the coloration of the background matched and obscured the tumor. In (b) the small size of the tumor caused it to be overlooked with photography. In (c) a bright retinal reflex in an 18-year-old patient made the tumor invisible with photography, but it could still be detected with OCTA. (d) shows a relapse of a hemangioblastoma in a retinal scar that, due to dark pigmentation of the pre-treated area, made the tumor obscure during clinical examination. OCTA revealed the relapse of the tumor as well as an additional primary tumor being hidden in the photograph due to the reddish background of the choroid. With permission from (Lang et al., 2024). (For interpretation of the references to color in this figure legend, the reader is referred to the Web version of this article.)

spring from the fundamental advantages of the technology: its amenability to quantification, its volumetric nature, and its non-invasiveness. In combination, these mean that OCTA can monitor the treatment response for important pathologies including neovascularization (Huang et al., 2015) and could screen for important treatment indicators (You et al., 2019) better than existing alternatives. Actually, we believe that one of the main remaining barriers to the widespread adoption of OCTA in the clinic is the narrow field of view, precisely the issue that this review covers solutions for. Small fields of view negate the advantage that OCTA as in comparisons to allied imaging modalities for detecting and quantifying features in diseases in which such pathology occurs in the mid-periphery. Its utility is therefore relatively diminished for analysis of such prevalent conditions as DR.

There is reason to believe that widefield OCTA would be a valuable addition to the clinic. To effectively argue for clinical adoption though more studies are needed. In particular, we require more and larger studies demonstrating superior quantification for widefield OCTA in addition to conventional OCTA, demonstrating superior detection sensitivity for pathologic features, and demonstrating improvement in patient outcomes through use of the technology. We hope that this review can help make the case for completing this work.

5. Summary

While widefield OCTA faces numerous technical challenges, expanding its field of view presents significant advantages. These include improved detection of pathology, identification of additional treatment indicators, enhanced comparisons with other imaging modalities, and greater diagnostic accuracy. Larger fields of view also offer valuable benefits to basic, translational, and clinical research, as well as to routine clinical practice.

CRediT authorship contribution statement

Yali Jia: Writing – review & editing, Writing – original draft, Conceptualization. **Tristan T. Hormel:** Writing – original draft, Investigation. **Thomas S. Hwang:** Writing – review & editing. **An-Lun Wu:** Visualization, Investigation. **Guangru B. Liang:** Writing – review & editing, Visualization. **Yukun Guo:** Writing – review & editing. **Xiang Wei:** Writing – review & editing. **Shuibin Ni:** Writing – review &

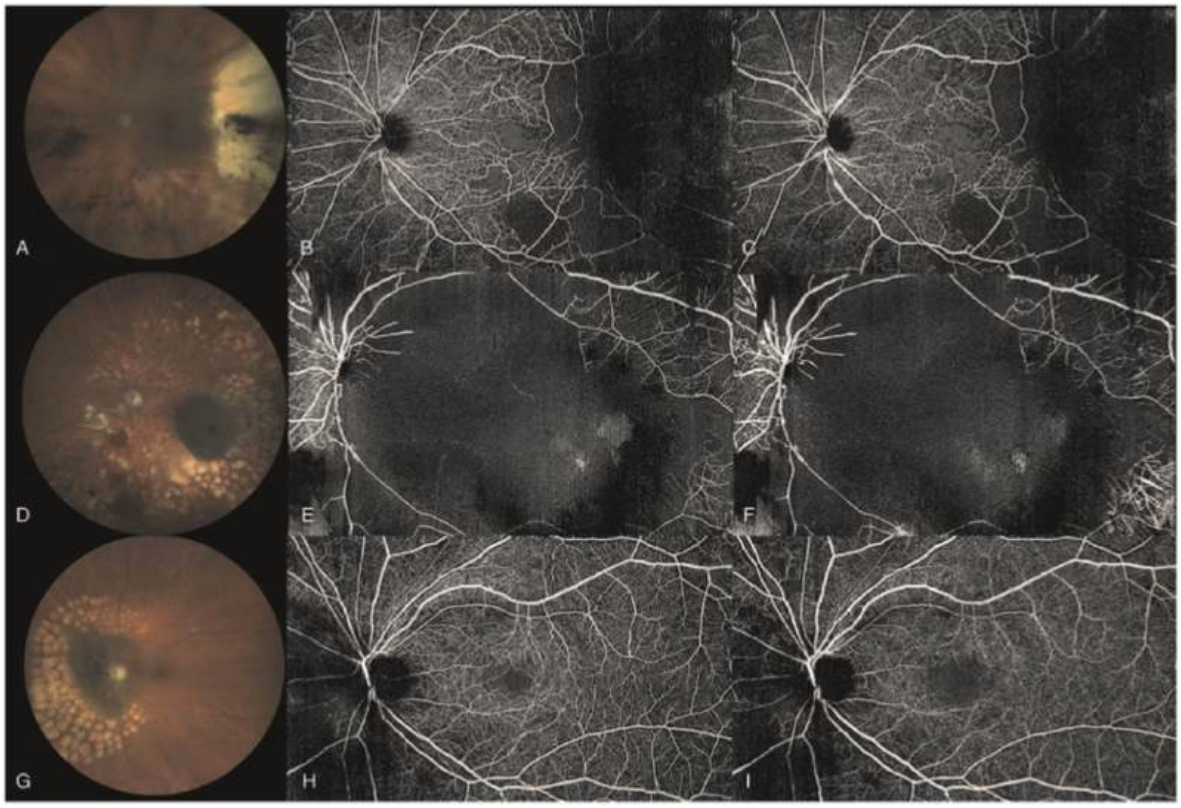

Fig. 25. Wide-field SS-OCTA in choroidal melanoma with clinically evident radiation retinopathy (CERR). A 70-year-old female, 10 years after plaque radiotherapy of a choroidal melanoma temporal to the macula, with telangiectasia inferior to the macular (A). Compared with the contralateral non-irradiated eye, there was ischemia in the region of the tumor, and discontinuity of the foveal avascular zone (FAZ) margin at the level of the superficial (B) and deep (C) capillary plexus. A 28-year-old male, 5 years after plaque radiotherapy of a choroidal melanoma in the temporal macular, with clinically evident proliferative radiation retinopathy (D). By SS-OCTA, there was severe ischemia with total loss of the parafoveal vasculature at the level of the superficial (E) and deep (F) plexuses. Wide-field swept-source optical coherence tomography angiography (SS-OCTA) in choroidal melanoma with no CERR. A 54-year-old male, 10 months after plaque radiotherapy of a peripapillary choroidal melanoma (G). Compared with the contralateral non-irradiated eye, at the level of the superficial capillary plexus, the FAZ margin was continuous but enlarged (H). Capillary dropout was present superior to the optic disc at the level of the deep capillary plexus (I).

editing. **Yifan Jian:** Writing – review & editing. **J. Peter Campbell:** Writing – review & editing. **Steven T. Bailey:** Writing – review & editing. **John C. Morrison:** Writing – review & editing. **David Huang:** Writing – review & editing.

Disclosures

Yali Jia: Optovue/Visionix, Inc. (P, R), Roche/Genentech, Inc. (P, R, F), Optos, Inc. (P), Boeringer Ingelheim Inc. (C), Ifocus Imaging (I); **Tristan T. Hormel**: Ifocus Imaging (I); **Thomas S. Hwang**: None; **An-Lun Wu**: None; **Guangru B. Liang**: None; **Yukun Guo**: None; **Xiang Wei**: None; **Shiubin Ni**: Siloam Vision (P); **Yifan Jian**: Siloam Vision (P, F); J. Peter Campbell: Siloam Vision (P, F); Boston AI Lab (C), Genentech (F) **Steven T. Bailey**: Visionix/Optovue, Inc. (F) **John C. Morrison**: None; **David Huang**: Visionix/Optovue, Inc. (F, P, R), Boeringer Ingelheim Inc. (C)

Funding

This work was supported by the National Institute of Health (R01 EY027833, R01 EY035410, R01 EY024544, R01 EY036429, R01 EY031394, R01 EY019474, R01 EY031331, R01 EY023285, R01 EY010145, R21 EY031883, T32 EY023211, UL1TR002369, P30 EY010572, P30 EY010572); the Malcolm M. Marquis, MD Endowed Fund for Innovation; an Unrestricted Departmental Funding Grant and Dr H. James and Carole Free Catalyst Award from Research to Prevent Blindness (NewYork, NY); Edward N. & Della L. Thome Memorial Foundation Award; and the Bright Focus Foundation (G2020168, M20230081).

Data availability

No data was used for the research described in the article.

References

Abtahi, M., Le, D., Lim, J.I., Yao, X., 2022. MF-AV-Net: an open-source deep learning network with multimodal fusion options for artery-vein segmentation in OCT angiography. Biomed. Opt. Express 13, 4870. https://doi.org/10.1364/boe.468483.

Abu-Qamar, O., Lewis, W., Mendonca, L.S.M., De Sisternes, L., Chin, A., Alibhai, A.Y., Gendelman, I., Reichel, E., Magazzeni, S., Kubach, S., Durbin, M., Witkin, A.J., Baumal, C.R., Duker, J.S., Waheed, N.K., 2023. Pseudoaveraging for denoising of OCT angiography: a deep learning approach for image quality enhancement in healthy and diabetic eyes. Int J Retina Vitreous 9. https://doi.org/10.1186/s40942-023-00486-5.

Aggarwal, K., Agarwal, A., Mahajan, S., Invernizzi, A., Mandadi, S.K.R., Singh, R., Bansal, R., Dogra, M.R., Gupta, V., 2018. The role of optical coherence tomography angiography in the diagnosis and management of acute Vogt–Koyanagi–Harada disease. Ocul. Immunol. Inflamm. 26, 142–153. https://doi.org/10.1080/09273948.2016.1195001.

Akkaya, I., Tozburun, S., 2022. A 1060 nm stretched-pulse mode-locked wavelength-swept laser source providing an A-scan rate of 20 MHz. Optik 266. https://doi.org/10.1016/j.ijleo.2022.169648.

An, L., Wang, R.K., 2008. In vivo volumetric imaging of vascular perfusion within human retina and choroids with optical micro-angiography. Opt. Express 16, 11438–11452. https://doi.org/10.1364/OE.16.011438.

Arya, M., Filho, M.B., Rebhun, C.B., Moult, E.M., Lee, B., Alibhai, Y., Witkin, A.J., Baumal, C.R., Duker, J.S., Fujimoto, J.G., Waheed, N.K., 2021. Analyzing relative flow speeds in diabetic retinopathy using variable interscan time analysis OCT

angiography. Ophthalmol Retina 5, 49–59. https://doi.org/10.1016/j.oret.2020.06.024.
Attendu, X., Ruis, R.M., 2019. Simple and robust calibration procedure for k-linearization and dispersion compensation in optical coherence tomography. J. Biomed. Opt. 24, 1. https://doi.org/10.1117/1.jbo.24.5.056001.
Balaratnasingam, C., An, D., Freund, K.B., Francke, A., Yu, D.-Y., 2019. Correlation between histologic and OCT angiography analysis of macular circulation. Ophthalmology 126, 1588–1589.
Bearelly, S., Rao, S., Fekrat, S., 2009. Anaphylaxis following intravenous fluorescein angiography in a vitreoretinal clinic: report of 4 cases. Can. J. Ophthalmol. 44, 444–445. https://doi.org/10.3129/i09-068.
Bistour, A., Mehanna, C.J., Chuttarsing, B., Colantuono, D., Amoroso, F., Beaumont, W., Matri, K. El, Souied, E.H., Miere, A., 2023. Widefield oct-angiography-based classification of sickle cell retinopathy. Graefe's Arch. Clin. Exp. Ophthalmol. 261, 2805–2812. https://doi.org/10.1007/s00417-023-06115-z.
Biswas, J., Sharma, T., Gopal, L., Madhavan, H.N., Sulochana, K.N., Ramakrishnan, S., 2002. Eales disease-an update. Surv. Ophthalmol. 47.
Biswas, S., Wan, K.H., 2019. Review of rodent hypertensive glaucoma models. Acta Ophthalmol. https://doi.org/10.1111/aos.13983.
Braaf, B., Vienola, K.V., Sheehy, C.K., Yang, Q., Vermeer, K.A., Tiruveedhula, P., Arathorn, D.W., Roorda, A., de Boer, J.F., 2013. Real-time eye motion correction in phase-resolved OCT angiography with tracking SLO. Biomed. Opt. Express 4, 51. https://doi.org/10.1364/boe.4.000051.
Branch Vein Occlusion Study Group, 1986. Argon laser scatter photocoagulation for prevention of neovascularization and vitreous hemorrhage in branch vein occlusion: a randomized clinical trial. Arch. Ophthalmol. 104, 34–41. https://doi.org/10.1001/archopht.1986.01050130044017.
Camino, A., Jia, Y., Liu, G., Wang, J., Huang, D., 2017. Regression-based algorithm for bulk motion subtraction in optical coherence tomography angiography. Biomed. Opt. Express 8, 3053–3066. https://doi.org/10.1364/BOE.8.003053.
Camino, A., Jia, Y., Yu, J., Wang, J., Liu, L., Huang, D., 2019. Automated detection of shadow artifacts in optical coherence tomography angiography. Biomed. Opt. Express 10, 1514–1531. https://doi.org/10.1364/BOE.10.001514.
Camino, A., Zhang, M., Gao, S.S., Hwang, T.S., Sharma, U., Wilson, D.J., Huang, D., Jia, Y., 2016. Evaluation of artifact reduction in optical coherence tomography angiography with real-time tracking and motion correction technology. Biomed. Opt. Express 7, 3905–3915. https://doi.org/10.1364/boe.7.003905.
Camino, A., Zhang, M., Liu, L., Wang, J., Jia, Y., Huang, D., 2018. Enhanced quantification of retinal perfusion by improved discrimination of blood flow from bulk motion signal in OCTA. Transl. Vis. Sci. Technol. 7. https://doi.org/10.1167/tvst.7.6.20.
Campbell, J. Peter, Nudleman, E., Yang, J., Tan, O., Chan, R.V.P., Chiang, M.F., Huang, D., Liu, G., 2017a. Handheld optical coherence tomography angiography and ultra–wide-field optical coherence tomography in retinopathy of prematurity. JAMA Ophthalmol 135.
Campbell, J. Peter, Nudleman, E., Yang, J., Tan, O., Chan, R.V.P., Chiang, M.F., Huang, D., Liu, G., 2017b. Handheld optical coherence tomography angiography and ultra-wide-field optical coherence tomography in retinopathy of prematurity. JAMA Ophthalmol 135, 977–981. https://doi.org/10.1001/jamaophthalmol.2017.2481.
Campbell, J.P., Zhang, M., Hwang, T.S., Bailey, S.T., Wilson, D.J., Jia, Y., Huang, D., 2017c. Detailed vascular anatomy of the human retina by projection-resolved optical coherence tomography angiography. Sci. Rep. 7, 1–11. https://doi.org/10.1038/srep42201.
Carlyle, W.C., Mcclain, J.B., Tzafriri, A.R., Bailey, L., Brett, G., Markham, P.M., Stanley, J.R.L., Edelman, E.R., Sciences, C.B., Technologies, E., Park, L.T., 2015. Optical coherence tomography angiography in choroideremia: correlating choriocapillaris loss with overlying degeneration. JAMA Ophthalmol 134 (Enhanced), 697–702. https://doi.org/10.1016/j.jconrel.2012.07.004.
Chaaya, C., Ploumi, I., Pandiri, S., Ding, X., Hoyek, S., Chen, C., Nodecker, K.N., Kim, A., Patel, N.A., Miller, J.B., 2025. Ultra widefield swept source OCTA findings in Coats plus syndrome. Ophthalmic Surg Lasers Imaging Retina 1–5. https://doi.org/10.3928/23258160-20250417-02.
Chen, S., Potsaid, B., Li, Y., Lin, J., Hwang, Y., Moult, E.M., Zhang, J., Huang, D., Fujimoto, J.G., 2022. High speed, long range, deep penetration swept source OCT for structural and angiographic imaging of the anterior eye. Sci. Rep. 12. https://doi.org/10.1038/s41598-022-04784-0.
Chen, X., Imperio, R., Viehland, C., Patel, P.R., Tran-Viet, D., Mangalesh, S., Prakalapakorn, S.G., Freedman, S.F., Izatt, J.A., Toth, C.A., 2024. A pilot optical coherence tomography angiography classification of retinal neovascularization in retinopathy of prematurity. Sci. Rep. 14. https://doi.org/10.1038/s41598-023-49964-8.
Chen, X., Niemeijer, M., Zhang, L., Lee, K., Abramoff, M.D., Sonka, M., 2012. Three-dimensional segmentation of fluid-associated abnormalities in retinal OCT: probability constrained graph-search-graph-cut. IEEE Trans. Med. Imag. 31, 1521–1531. https://doi.org/10.1109/TMI.2012.2191302.
Cheng, L., Chen, X., Weng, S., Mao, L., Gong, Y., Yu, S., Xu, X., 2016. Spectral-domain optical coherence tomography angiography findings in multifocal choroiditis with active lesions. Am. J. Ophthalmol. 169, 145–161. https://doi.org/10.1016/j.ajo.2016.06.029.
Cheng, Y., Chu, Z., Wang, R.K., 2021. Robust three-dimensional registration on optical coherence tomography angiography for speckle reduction and visualization. Quant. Imag. Med. Surg. 11, 879–894. https://doi.org/10.21037/QIMS-20-751.
Choma, M.A., Hsu, K., Izatt, J.A., 2005. Swept source optical coherence tomography using an all-fiber 1300-nm ring laser source. J. Biomed. Opt. 10, 044009. https://doi.org/10.1117/1.1961474.
Choma, M.A., Sarunic, M.V., Yang, C., Izatt, J.A., 2003. Sensitivity advantage of swept source and Fourier domain optical coherence tomography. Opt. Express 11, 2183–2189.
Choudhry, N., Duker, J.S., Freund, K.B., Kiss, S., Querques, G., Rosen, R., Sarraf, D., Souied, E.H., Stanga, P.E., Staurenghi, G., Sadda, S.V.R., 2019. Classification and guidelines for widefield imaging: recommendations from the International widefield imaging study group. Ophthalmol Retina 3, 843–849. https://doi.org/10.1016/j.oret.2019.05.007.
Clarke, K., Mannath, A., Anastasi, M., Nasr, M., Pan, S., Balaskas, K., Dinah, C., Sarunic, M.V., Asaria, R., 2025. Optical coherence tomography angiography as a tool for diagnosis and monitoring of sickle cell related eye disease: a systematic review and meta-analysis. Eye (Basingstoke). https://doi.org/10.1038/s41433-025-03814-1.
Conway, J.E., Chou, D., Clatterbuck, R., Brem, H., Long, D., 2001. Hemangioblastomas of the Central Nervous System in von Hippel-Lindau Syndrome and Sporadic Disease. Neurosurgery 48.
Couturier, A., Rey, P.A., Erginay, A., Lavia, C., Bonnin, S., Dupas, B., Gaudric, A., Tadayoni, R., 2019. Widefield OCT-angiography and fluorescein angiography assessments of nonperfusion in diabetic retinopathy and edema treated with anti–vascular Endothelial growth factor. Ophthalmology 126, 1685–1694. https://doi.org/10.1016/j.ophtha.2019.06.022.
Cui, Y., Zhu, Y., Wang, J.C., Lu, Y., Zeng, R., Katz, R., Vingopoulos, F., Le, R., Laíns, I., Wu, D.M., Eliott, D., Vavvas, D.G., Husain, D., Miller, J.W., Kim, L.A., Miller, J.B., 2021. Comparison of widefield swept-source optical coherence tomography angiography with ultra-widefield colour fundus photography and fluorescein angiography for detection of lesions in diabetic retinopathy. Br. J. Ophthalmol. 105, 577–581. https://doi.org/10.1136/bjophthalmol-2020-316245.
Dai, L., Huang, F., Jiang, Q., Guo, S., Tan, S., Su, G., Yang, P., 2024. Sensitive optical coherence tomography angiography parameters detecting retinal vascular changes in Behcet's uveitis. Photodiagnosis Photodyn. Ther. 49. https://doi.org/10.1016/j.pdpdt.2024.104353.
De Pretto, L.R., Moult, E.M., Alibhai, A.Y., Carrasco-Zevallos, O.M., Chen, S., Lee, B.K., Witkin, A.J., Baumal, C.R., Reichel, E., de Freitas, A.Z., Duker, J.S., Waheed, N.K., Fujimoto, J.G., 2019. Controlling for artifacts in widefield optical coherence tomography angiography measurements of non-perfusion area. Sci. Rep. 9, 1–15. https://doi.org/10.1038/s41598-019-43958-1.
de Smet, M.D., Taylor, S.R.J., Bodaghi, B., Miserocchi, E., Murray, P.I., Pleyer, U., Zierhut, M., Barisani-Asenbauer, T., LeHoang, P., Lightman, S., 2011. Understanding uveitis: the impact of research on visual outcomes. Prog. Retin. Eye Res. https://doi.org/10.1016/j.preteyeres.2011.06.005.
Decker, N.L., Duffy, B.V., Boughanem, G.O., Fukuyama, H., Castellanos Canales, D., Nesper, P.L., Gill, M.K., Fawzi, A.A., 2023. Macular perfusion deficits on OCTA correlate with non-perfusion on ultrawide-field FA in diabetic retinopathy. Ophthalmol Retina. https://doi.org/10.1016/j.oret.2023.04.003.
Di Pierdomenico, J., Henderson, D.C.M., Giammaria, S., Smith, V.L., Jamet, A.J., Smith, C.A., Hooper, M.L., Chauhan, B.C., 2022. Age and intraocular pressure in murine experimental glaucoma. Prog. Retin. Eye Res. https://doi.org/10.1016/j.preteyeres.2021.101021.
Ditchburn, R.W., Ginsborg, B.L., 1953. Involuntary eye movements during fixation. J. Physiol 119.
Duh, E.J., Sun, J.K., Stitt, A.W., 2017. Diabetic retinopathy: current understanding, mechanisms, and treatment strategies. JCI Insight 2, 1–13. https://doi.org/10.1172/jci.insight.93751.
Duma, V.-F., Tankam, P., Huang, J., Won, J., Rolland, J.P., 2015. Effective duty cycle of galvanometer-based scanners: impact on OCT imaging. In: Design and Quality for Biomedical Technologies VIII, p. 93150J. https://doi.org/10.1117/12.2079776. SPIE.
Fan, W., Wang, K., Ghasemi Falavarjani, K., Sagong, M., Uji, A., Ip, M., Wykoff, C.C., Brown, D.M., van Hemert, J., Sadda, S.V.R., 2017. Distribution of nonperfusion area on ultra-widefield fluorescein angiography in eyes with diabetic macular edema: DAVE study. Am. J. Ophthalmol. 180, 110–116. https://doi.org/10.1016/j.ajo.2017.05.024.
Feke, G.T., Tagawa, H., Deupree, D.M., Goger, D.G., Sebog, J., Weirer, J.J., 1989. Blood flow in the normal human retina. Investig. Ophthalmol. Vis. Sci. 30.
Fierson, W.M., 2018. Screening examination of premature infants for retinopathy of prematurity. Pediatrics 142.
Flynn Roberts, M., Fishman, G.A., Roberts, D.K., Heckenlively, J.R., Weleber, R.G., Anderson, R.J., Grover, S., 2002. Retrospective, longitudinal, and cross sectional study of visual acuity impairment in choroideraemia. Br. J. Ophthalmol. 86, 658–662.
Forte, P., Paques, M., Cattaneo, J., Dupas, B., Castro-Farias, D., Girmens, J.F., Siab, M., Biagini, F., Nicolò, M., Eandi, C.M., Sacconi, R., Querques, G., 2025. Perifoveal vascular anomalous complex and telangiectatic capillaries: an overview of two entities potentially sharing a common pathophysiology. Surv. Ophthalmol. https://doi.org/10.1016/j.survophthal.2025.01.007.
Francis, P.J., Appukuttan, B., Simmons, E., Landauer, N., Stoddard, J., Hamon, S., Ott, J., Ferguson, B., Klein, M., Stout, J.T., Neuringer, M., 2008. Rhesus monkeys and humans share common susceptibility genes for age-related macular disease. Hum. Mol. Genet. 17, 2673–2680. https://doi.org/10.1093/hmg/ddn167.
Fruttiger, M., 2002. Development of the mouse retinal vasculature: Angiogenesis versus Vasculogenesis. Investig. Ophthalmol. Vis. Sci. 43, 522–527.
Gao, M., Guo, Y., Hormel, T.T., Sun, J., Hwang, T.S., Jia, Y., 2020. Reconstruction of high-resolution 6×6-mm OCT angiograms using deep learning. Biomed. Opt. Express 11, 3585. https://doi.org/10.1364/boe.394301.
Gao, M., Guo, Y., Hormel, T.T., Tsuboi, K., Pacheco, G., Poole, D., Bailey, S.T., Flaxel, C. J., Huang, D., Hwang, T.S., Jia, Y., 2022a. A deep learning network for classifying

Arteries and veins in montaged widefield OCT angiograms. Ophthalmology Science 2, 100149. https://doi.org/10.1016/j.xops.2022.100149.
Gao, M., Hormel, T., Guo, Y., Bailey, S.T., Flaxel, C.J., Huang, D., Hwang, T.S., Jia, Y., 2022b. Identification and characterization of microaneurysm in OCT and OCT angiography. Investig. Ophthalmol. Vis. Sci. 63.
Gao, M., Hormel, T.T., Guo, Y., Tsuboi, K., Flaxel, C.J., Huang, D., Hwang, T.S., Jia, Y., 2024. Perfused and nonperfused microaneurysms identified and characterized by structural and angiographic OCT. Ophthalmol Retina 8, 108–115. https://doi.org/10.1016/j.oret.2023.08.019.
Gao, M., Hormel, T.T., Wang, J., Guo, Y., Bailey, S.T., Hwang, T.S., Jia, Y., 2021. An open-source deep learning network for reconstruction of high-resolution oct angiograms of retinal intermediate and deep capillary plexuses. Transl. Vis. Sci. Technol. 10, 1–14. https://doi.org/10.1167/TVST.10.13.13.
Gao, S.S., Patel, R.C., Jain, N., Zhang, M., Weleber, R.G., Huang, D., Pennesi, M.E., 2017. Choriocapillaris evaluation in choroideremia using optical coherence tomography angiography. Biomed. Opt. Express 8, 48–56.
García-Aparicio, Á., García de Yébenes, M.J., Otón, T., Muñoz-Fernández, S., 2021. Prevalence and incidence of uveitis: a systematic review and meta-analysis. Ophthalmic Epidemiol. https://doi.org/10.1080/09286586.2021.1882506.
Glacet-Bernard, A., Miere, A., Houmane, B., Tilleul, J., Souied, E., 2021. NONPERFUSION assessment in retinal vein occlusion comparison between ultra-widefield fluorescein angiography and widefield optical coherence tomography angiography. Retina 41, 1202–1209.
Goldberg, M.F., 1971. Classification and pathogenesis of proliferative sickle retinopathy. Am. J. Ophthalmol. 71, 649–665. https://doi.org/10.1016/0002-9394(71)90429-6.
Gorczynska, I., Migacz, J.V., Jonnal, R., Zawadzki, R.J., Poddar, R., Werner, J.S., 2017. Imaging of the human choroid with a 1.7 MHz A-scan rate FDML swept source OCT system. Ophthalmic Technologies XXVII 10045, 1004510. https://doi.org/10.1117/12.2251704.
Gouras, P., Ivert, L., Landauer, N., Mattison, J.A., Ingram, D.K., Neuringer, M., 2008. Drusenoid maculopathy in rhesus monkeys (Macaca mulatta): effects of age and gender. Graefe's Arch. Clin. Exp. Ophthalmol. 246, 1395–1402. https://doi.org/10.1007/s00417-008-0910-8.
Greig, E.C., Laver, N.V., Mendonca, L.S.M., Levine, E.S., Baumal, C.R., Waheed, N.K., Duker, J.S., 2021. SWEPT-SOURCE optical coherence tomography angiography in small choroidal melanomas and choroidal nevi. Retina 41, 1182–1192. https://doi.org/10.1097/IAE.0000000000003053.
Grover, S., Fishman, G.A., Birch, D.G., Locke, K.G., Rosner, B., 2003. Variability of full-field electroretinogram photoreceptor cell disease. Ophthalmology 110, 1159–1163. https://doi.org/10.1016/S0161-6420(03)00253-7.
Guariguata, L., Whiting, D.R., Hambleton, I., Beagley, J., Linnenkamp, U., Shaw, J.E., 2014. Global estimates of diabetes prevalence for 2013 and projections for 2035. Diabetes Res. Clin. Pract. 103, 137–149. https://doi.org/10.1016/j.diabres.2013.11.002.
Guly, C.M., Forrester, J.V., 2010. Investigation and management of uveitis. BMJ (Online). https://doi.org/10.1136/bmj.c4976.
Guo, Y., Hormel, T.T., Gao, L., You, Q., Wang, B., Flaxel, C.J., Bailey, S.T., Choi, D., Huang, D., Hwang, T.S., Jia, Y., 2021. Quantification of nonperfusion area in montaged widefield OCT angiography using deep learning in diabetic retinopathy. Ophthalmology Science 1, 100027. https://doi.org/10.1016/j.xops.2021.100027.
Guo, Y., Hormel, T.T., Xiong, H., Wang, B., Camino, A., Wang, J., Huang, D., Hwang, T. S., Jia, Y., 2019. Development and validation of a deep learning algorithm for distinguishing the nonperfusion area from signal reduction artifacts on OCT angiography. Biomed. Opt. Express 10, 3257. https://doi.org/10.1364/boe.10.003257.
Hagag, A.M., Wang, J.I.E., Lu, K., Harman, G., Weleber, R.G., Huang, D., Yang, P., Pennesi, M.E., Jia, Y., 2019. Projection-resolved optical coherence tomographic angiography of retinal plexuses in retinitis pigmentosa. Am. J. Ophthalmol. 204, 70–79. https://doi.org/10.1016/j.ajo.2019.02.034.
Hariri, A.H., Zhang, H.Y., Ho, A., Francis, P., Weleber, R.G., Birch, D.G., Ferris, F.L., Sadda, S.V.R., Bernstein, P.S., Heckenlively, J., Iannaccone, A., Lam, B., Pennesi, M. E., Chiostri, J., Erker, L.R., Wilson, D.J., McCormack, J.B., 2016. Quantification of ellipsoid zone changes in retinitis pigmentosa using en face spectral domain-optical coherence tomography. JAMA Ophthalmol 134, 628–635. https://doi.org/10.1001/jamaophthalmol.2016.0502.
Hartong, D.T., Berson, E.L., Dryja, T.P., 2006. Retinitis pigmentosa. Lancet 368, 1795–1809.
Hellström, A., Smith, L.E.H., Dammann, O., 2013. Retinopathy of prematurity. In: The Lancet. Elsevier B.V., pp. 1445–1457. https://doi.org/10.1016/S0140-6736(13)60178-6
Hendargo, H.C., Estrada, R., Chiu, S.J., Tomasi, C., Farsiu, S., Izatt, J.A., 2013. Automated non-rigid registration and mosaicing for robust imaging of distinct retinal capillary beds using speckle variance optical coherence tomography. Biomed. Opt. Express 4, 803. https://doi.org/10.1364/boe.4.000803.
Henderson, R.H., 2019. Inherited retinal dystrophies. Pediatrics and Child Health 30.
Holopigian, K., Greenstein, V., Seiple, W., Carr, R.E., 1996. Rates of change differ among measures of visual function in patients with retinitis pigmentosa. Ophthalmology 103, 398–405. https://doi.org/10.1016/S0161-6420(96)30679-9.
Hormel, Tristan T., Huang, D., Jia, Y., 2021a. Artifacts and Artifact Removal in Optical Coherence Tomographic Angiography, vol. 11, pp. 1120–1133. https://doi.org/10.21037/qims-20-730.
Hormel, Tristan T., Hwang, T.S., Bailey, S.T., Wilson, D.J., Huang, D., Jia, Y., 2021b. Artificial intelligence in OCT angiography. Prog. Retin. Eye Res., 100965. https://doi.org/10.1016/j.preteyeres.2021.100965.
Hormel, Tristan T., Jia, Y., Jian, Y., Hwang, T.S., Bailey, S.T., Pennesi, M.E., Wilson, D.J., Morrison, J.C., Huang, D., 2021c. Plexus-specific retinal vascular anatomy and pathologies as seen by projection-resolved optical coherence tomographic angiography. Prog. Retin. Eye Res. 80, 100878. https://doi.org/10.1016/j.preteyeres.2020.100878.
Huang, D., Jia, Y., Rispoli, M., Tan, O., Lumbroso, B., 2015. Optical coherence tomography angiography of time course of choroidal neovascularization in response to anti-angiogenic treatment. Retina 35, 2260–2264. https://doi.org/10.1097/IAE.0000000000000846.
Huang, D., Li, F., He, Z., Cheng, Z., Shang, C., Wai, P.K.A., 2020. 400 MHz ultrafast optical coherence tomography. Opt Lett 45, 6675. https://doi.org/10.1364/ol.409607.
Huang, N., Hormel, T., Liang, G., Wei, X., Guo, Y., Chen, S., Jia, Y., 2024. Optimizing numerical k-sampling for swept-source optical coherence tomography angiography. Opt Lett 49. https://doi.org/10.1364/ol.518720.
Huang, X.F., Brown, M.A., 2022. Progress in the genetics of uveitis. Genes Immun. https://doi.org/10.1038/s41435-022-00168-6.
Huber, R., Wojtkowski, M., Fujimoto, J.G., 2006. Fourier Domain Mode Locking (FDML): a new laser operating regime and applications for optical coherence tomography. Opt. Express 254, 3225–3237.
Huemer, J., Khalid, H., Wagner, S.K., Nicholson, L., Fu, D.J., Sim, D.A., Patel, P.J., Balaskas, K., Rajendram, R., Keane, P.A., 2021. Phenotyping of retinal neovascularization in ischemic retinal vein occlusion using wide field OCT angiography. Eye (Basingstoke) 35, 2812–2819. https://doi.org/10.1038/s41433-020-01317-9.
Hughes, A., 1979. A schematic eye for the rat. Vis. Res. 19, 263–278. https://doi.org/10.1016/0042-6989(79)90172-X.
Hwang, T.S., Gao, S.S., Liu, L., Lauer, A.K., Bailey, S.T., Flaxel, C.J., Wilson, D.J., Huang, D., Jia, Y., 2016. Automated quantification of capillary nonperfusion using optical coherence tomography angiography in diabetic retinopathy. JAMA Ophthalmol 134, 367–373. https://doi.org/10.1001/jamaophthalmol.2015.5658.
Hwang, T.S., Hagag, A.M., Wang, J., Zhang, M., Smith, A., Wilson, D.J., Huang, D., Jia, Y., 2018. Automated quantification of nonperfusion areas in 3 vascular plexuses with optical coherence tomography angiography in eyes of patients with diabetes. JAMA Ophthalmol 136, 929–936. https://doi.org/10.1001/jamaophthalmol.2018.2257.
Hwang, T.S., Jia, Y., Gao, S.S., Bailey, S.T., Lauer, A.K., Flaxel, C.J., Wilson, D.J., Huang, D., 2015. Optical coherence tomography angiography features in diabetic retionopathy. Retina 35, 2371–2376. https://doi.org/10.1097/IAE.0000000000000716.
Iadecola, C., 2017. The Neurovascular unit coming of age: a journey through Neurovascular coupling in health and disease. Neuron 96, 17–42. https://doi.org/10.1016/j.neuron.2017.07.030.
Ito, H., Ito, Y., Kataoka, K., Ueno, S., Takeuchi, J., Nakano, Y., Fujita, A., Horiguchi, E., Kaneko, H., Iwase, T., Terasaki, H., 2020. Association between retinal layer thickness and perfusion status in Extramacular areas in diabetic retinopathy. Am. J. Ophthalmol. 215, 25–36. https://doi.org/10.1016/j.ajo.2020.03.019.
Jain, N., Jia, Y., Gao, S.S., Zhang, X., Weleber, R.G., Huang, D., Pennesi, M.E., 2016. Optical coherence tomography angiography in choroideremia correlating choriocapillaris loss with overlying degeneration. JAMA Ophthalmol 134, 1–6. https://doi.org/10.1001/jamaophthalmol.2016.0874.
Jaulim, A., Ahmed, B., Khanam, T., Chatziralli, I.P., 2013. Branch retinal vein occlusion: epidemiology, pathogenesis, and complications. An update of the literature. Retina 33.
Jia, Y., Tan, O., Tokayer, J., Potsaid, B., Wang, Y., Liu, J.J., Kraus, M.F., Subhash, H., Fujimoto, J.G., Hornegger, J., Huang, D., 2012. Split-spectrum amplitude-decorrelation angiography with optical coherence tomography. Opt. Express 20, 4710–4725. https://doi.org/10.1364/OE.20.004710.
John, D.D., Burgner, C.B., Potsaid, B., Robertson, M.E., Lee, B.K., Choi, W.J., Cable, A.E., Fujimoto, J.G., Jayaraman, V., 2015. Wideband electrically pumped 1050-nm MEMS-tunable VCSEL for ophthalmic imaging. J. Lightwave Technol. 33, 3461–3468. https://doi.org/10.1109/JLT.2015.2397860.
Ju, M.J., Heisler, M., Athwal, A., Sarunic, M.V., Jian, Y., 2018. Effective bidirectional scanning pattern for optical coherence tomography angiography. Biomed. Opt. Express 9, 2336. https://doi.org/10.1364/boe.9.002336.
Jung, J.J., Chen, M.H., Frambach, C.R., Rofagha, S., Lee, S.S., 2018. Spectral domain versus swept source optical coherence tomography angiography of the retinal capillary plexuses in sickle cell maculopathy. Retin. Cases Brief Rep. 12, 87–92. https://doi.org/10.1097/ICB.0000000000000448.
Kadomoto, S., Muraoka, Y., Uji, A., Tamiya, R., Oritani, Y., Kawai, K., Ooto, S., Murakami, T., Iida-Miwa, Y., Tsujikawa, A., 2021. NONPERFUSION area quantification in branch retinal vein occlusion A widefield optical coherence tomography angiography study. Retina 41, 1210–1218.
Kang, J., Feng, P., Wei, X., Lam, E.Y., Tsia, K.K., Wong, K.K.Y., 2018. 102-nm, 445-MHz inertial-free swept source by mode-locked fiber laser and time stretch technique for optical coherence tomography. Opt. Express 26, 4370. https://doi.org/10.1364/oe.26.004370.
Kim, A.Y., Rodger, D.C., Shahidzadeh, A., Chu, Z., Koulisis, N., Burkemper, B., Jiang, X., Pepple, K.L., Wang, R.K., Puliafito, C.A., Rao, N.A., Kashani, A.H., 2016. Quantifying retinal microvascular changes in uveitis using spectral-domain optical coherence tomography angiography. Am. J. Ophthalmol. 171, 101–112. https://doi.org/10.1016/j.ajo.2016.08.035.
Klein, T., Wieser, W., Eigenwillig, C.M., Biedermann, B.R., Huber, R., 2011. Megahertz OCT for ultrawide-field retinal imaging with a 1050nm Fourier domain mode-locked laser. Opt. Express 19, 3044. https://doi.org/10.1364/oe.19.003044.
Klufas, M.A., Phasukkijwatana, N., Iafe, N.A., Prasad, P.S., Agarwal, A., Gupta, V., Ansari, W., Pichi, F., Srivastava, S., Freund, K.B., Sadda, S.V.R., Sarraf, D., 2017. Optical coherence tomography angiography reveals choriocapillaris flow reduction

in Placoid chorioretinitis. Ophthalmol Retina 1, 77–91. https://doi.org/10.1016/j.oret.2016.08.008.
Kolb, J.P., Klein, T., Kufner, C.L., Wieser, W., Neubauer, A.S., Huber, R., 2015. Ultra-widefield retinal MHz-OCT imaging with up to 100 degrees viewing angle. Biomed. Opt. Express 6, 1534–1552. https://doi.org/10.1364/BOE.6.001534.
Kornblau, I.S., El-Annan, J.F., 2019. Adverse reactions to fluorescein angiography: a comprehensive review of the literature. Surv. Ophthalmol. https://doi.org/10.1016/j.survophthal.2019.02.004.
Koyanagi, Y., Murakami, Y., Funatsu, J., Akiyama, M., Nakatake, S., Fujiwara, K., Tachibana, T., Nakao, S., Hisatomi, T., Yoshida, S., Ishibashi, T., Sonoda, K.H., Ikeda, Y., 2018. Optical coherence tomography angiography of the macular microvasculature changes in retinitis pigmentosa. Acta Ophthalmol. 96, e59–e67. https://doi.org/10.1111/aos.13475.
Lang, S.J., Dreesbach, M., Laich, Y., Glatz, A., Boehringer, D., Grewing, V., Fritz, M., Bucher, F., Lagrèze, W.A., Maloca, P.M., Reinhard, T., Lange, C., Agostini, H., Reich, M., 2024. ZEISS PLEX Elite 9000 Widefield Optical Coherence Tomography Angiography as Screening Method for Early Detection of Retinal Hemangioblastomas in von Hippel–Lindau Disease. Transl. Vis. Sci. Technol. 13. https://doi.org/10.1167/tvst.13.2.8.
Lauermann, J.L., Treder, M., Alnawaiseh, M., Clemens, C.R., Eter, N., Alten, F., 2019. Automated OCT angiography image quality assessment using a deep learning algorithm. Graefe's Arch. Clin. Exp. Ophthalmol. 257, 1641–1648. https://doi.org/10.1007/s00417-019-04338-7.
Lee, K.K.C., Mariampillai, A., Yu, J.X.Z., Cadotte, D.W., Wilson, B.C., Standish, B.A., Yang, V.X.D., 2012. Real-time speckle variance swept-source optical coherence tomography using a graphics processing unit. Biomed. Opt. Express 3, 14685–14704.
Lee, Y.J., Sun, S., Kim, Y.K., Jeoung, J.W., Park, K.H., 2023. Diagnostic ability of macular microvasculature with swept-source OCT angiography for highly myopic glaucoma using deep learning. Sci. Rep. 13. https://doi.org/10.1038/s41598-023-32164-9.
Leung, C.K.S., Cheung, C.Y.L., Weinreb, R.N., Qiu, K., Liu, S., Li, H., Xu, G., Fan, N., Pang, C.P., Tse, K.K., Lam, D.S.C., 2010. Evaluation of retinal nerve fiber layer progression in glaucoma: a study on optical coherence tomography guided progression analysis. Investig. Ophthalmol. Vis. Sci. 51, 217–222. https://doi.org/10.1167/iovs.09-3468.
Levison, A.L., Baynes, K.M., Lowder, C.Y., Kaiser, P.K., Srivastava, S.K., 2017. Choroidal neovascularisation on optical coherence tomography angiography in punctate inner choroidopathy and multifocal choroiditis. Br. J. Ophthalmol. 101, 616–622. https://doi.org/10.1136/bjophthalmol-2016-308806.
Li, J., Wei, D., Mao, M., Li, M., Liu, S., Li, F., Li, C., Liu, M., Leng, H., Wang, Y., Ning, X., Liu, Y., Dong, W., Zhong, J., 2022. Ultra-widefield color fundus photography combined with high-speed ultra-widefield swept-source optical coherence tomography angiography for non-invasive detection of lesions in diabetic retinopathy. Front. Public Health 10, 1047608.
Liang, G.B., Hormel, T.T., Wei, X., Guo, Y., Wang, J., Hwang, T., Jia, Y., 2023. Single-shot OCT and OCT angiography for slab-specific detection of diabetic retinopathy. Biomed. Opt. Express 14, 5682. https://doi.org/10.1364/boe.503476.
Liang, G.B., Ni, S., Hormel, T.T., Morrison, J.C., Lozano, D.C., Campbell, J.P., Jia, Y., 2024. 112° field of view high-resolution swept-source OCT angiography for rat retinas. Opt Lett.
Lim, L.A.S., Camp, D.A., Ancona-Lezama, D., Mazloumi, M., Patel, S.P., McLaughlin, J. W., Ferenczy, S.R., Mashayekhi, A., Shields, C.L., 2020. Wide-field (15× 9mm) swept-source optical coherence tomography angiography following plaque radiotherapy of choroidal melanoma: an analysis of 105 eyes. Asia-Pacific Journal of Ophthalmology 9, 326–334. https://doi.org/10.1097/APO.0000000000000282.
Liu, G., Jia, Y., Pechauer, A.D., Chandwani, R., Huang, D., 2016. Split-spectrum phase-gradient optical coherence tomography angiography. Biomed. Opt. Express 7, 2943–2954.
Madan, A., Penn, J.S., 2003. Animal models of oxygen-induced retinopathy. Front. Biosci. 84, A7–A9. https://doi.org/10.1016/s0003-9993(03)00458-1.
Makita, S., Hong, Y., Yamanari, M., Yatagai, T., Yasuno, Y., 2006. Optical coherence angiography. Opt. Express 14, 7821–7840. https://doi.org/10.1364/OE.14.007821.
Mase, T., Ishibazawa, A., Nagaoka, T., Yokota, H., Yoshida, A., 2016. Radial peripapillary capillary network visualized using wide-field montage optical coherence tomography angiography. Investig. Ophthalmol. Vis. Sci. 57, 504–510. https://doi.org/10.1167/iovs.15-18877.
Massin, P., Duguid, G., Erginay, A., Haouchine, B., Gaudric, A., 2003. Optical coherence tomography for evaluating diabetic macular edema before and after vitrectomy. Am. J. Ophthalmol. 135, 169–177. https://doi.org/10.1016/S0002-9394(02)01837-8.
Mastropasqua, R., D'Aloisio, R., De Nicola, C., Ferro, G., Senatore, A., Libertini, D., Di Marzio, G., Di Nicola, M., Di Martino, G., Di Antonio, L., Toto, L., 2020. Widefield swept source OCTA in retinitis pigmentosa. Diagnostics 10. https://doi.org/10.3390/diagnostics10010050.
McBride, J.L., Neuringer, M., Ferguson, B., Kohama, S.G., Tagge, I.J., Zweig, R.C., Renner, L.M., McGill, T.J., Stoddard, J., Peterson, S., Su, W., Sherman, L.S., Domire, J.S., Ducore, R.M., Colgin, L.M., Lewis, A.D., 2018. Discovery of a CLN7 model of Batten disease in non-human primates. Neurobiol. Dis. 119, 65–78. https://doi.org/10.1016/j.nbd.2018.07.013.
Mehta, N., Cheng, Y., Yasin Alibhai, A., Duker, J.S., Wang, R.K., Waheed, N.K., 2021. Optical coherence tomography angiography distortion correction in widefield montage images. Quant. Imag. Med. Surg. 11, 928–938. https://doi.org/10.21037/QIMS-20-791.
Mezu-Ndubuisi, O.J., Teng, P. yu, Wanek, J., Blair, N.P., Chau, F.Y., Reddy, N.M., Raj, J. U., Reddy, S.P., Shahidi, M., 2013. In vivo retinal vascular oxygen tension imaging and fluorescein angiography in the mouse model of oxygen-induced retinopathy. Investig. Ophthalmol. Vis. Sci. 54, 6968–6972. https://doi.org/10.1167/iovs.13-12126.
Miao, Y., Siadati, M., Song, J., Ma, D., Jian, Y., Beg, M.F., Sarunic, M.V., Ju, M.J., 2021. Phase-corrected buffer averaging for enhanced OCT angiography using FDML laser. Opt Lett 46, 3833. https://doi.org/10.1364/ol.430915.
Miserocchi, E., Fogliato, G., Modorati, G., Bandello, F., 2013. Review on the worldwide epidemiology of uveitis. Eur. J. Ophthalmol. 23, 705–717. https://doi.org/10.5301/ejo.5000278.
Mookiah, M.R.K., Acharya, U.R., Fujita, H., Tan, J.H., Chua, C.K., Bhandary, S.V., Laude, A., Tong, L., 2015. Application of different imaging modalities for diagnosis of Diabetic Macular Edema: a review. Comput. Biol. Med. 66, 295–315. https://doi.org/10.1016/j.compbiomed.2015.09.012.
Moon, S., Chen, Z., 2018. Phase-stability optimization of swept-source optical coherence tomography. Biomed. Opt. Express 9, 5280. https://doi.org/10.1364/boe.9.005280.
Morrison, J.C., Moore, C.G., H Deppmeier, L.M., Gold, B.G., Meshul, C.K., Johnson, E.C., 1997. A rat model of chronic pressure-induced optic nerve damage. Exp. Eye Res.
Munk, M.R., Kashani, A.H., Tadayoni, R., Korobelnik, J.F., Wolf, S., Pichi, F., Koh, A., Ishibazawa, A., Gaudric, A., Loewenstein, A., Lumbroso, B., Ferrara, D., Sarraf, D., Wong, D.T., Skondra, D., Rodriguez, F.J., Staurenghi, G., Pearce, I., Kim, J.E., Freund, K.B., Parodi, M.B., Waheed, N.K., Rosen, R., Spaide, R.F., Nakao, S., Sadda, S.V., Vujosevic, S., Wong, T.Y., Murata, T., Chakravarthy, U., Ogura, Y., Huf, W., Tian, M., 2022. Recommendations for OCT angiography reporting in retinal vascular disease: a Delphi approach by International experts. Ophthalmol Retina 6, 753–761. https://doi.org/10.1016/j.oret.2022.02.007.
Murakami, Y., Ikeda, Y., Akiyama, M., Fujiwara, K., Yoshida, N., Notomi, S., Nabeshima, T., Hisatomi, T., Enaida, H., Ishibashi, T., 2014. Correlation between macular blood flow and central visual sensitivity in retinitis pigmentosa. Acta Ophthalmol. 93, 644–648. https://doi.org/10.1111/aos.12693.
Nakamura, K., Akiyama, H., Tokui, S., Saito, K., Nitta, K., 2024. A case of eales disease observed by widefield optical coherence tomography angiography. Retin. Cases Brief Rep. 18, 116–119.
Nesper, P.L., Fawzi, A.A., 2022. New method for reducing Artifactual flow deficits caused by compensation techniques in the choriocapillaris with optical coherence tomography angiography. Retina 42, 328–335. https://doi.org/10.1097/IAE.0000000000003313.
Nguyen, T.T.P., Ni, S., Liang, G., Khan, S., Wei, X., Skalet, A., Ostmo, S., Chiang, M.F., Jia, Y., Huang, D., Jian, Y., Campbell, J.P., 2022. Widefield optical coherence tomography in pediatric retina: a case series of Intraoperative applications using a Prototype handheld device. Front. Med. 9. https://doi.org/10.3389/fmed.2022.860371.
Ni, S., Liang, G. Ben, Ng, R., Ostmo, S., Jia, Y., Chiang, M.F., Huang, D., Skalet, A.H., Young, B.K., Campbell, J.P., Jian, Y., 2024. Panretinal handheld OCT angiography for pediatric retinal imaging. Biomed. Opt. Express 15, 3412. https://doi.org/10.1364/boe.520739.
Ni, S., Wei, X., Ng, R., Ostmo, S., Chiang, M.F., Huang, D., Jia, Y., Campbell, J.P., Jian, Y., 2021. High-speed and widefield handheld swept-source OCT angiography with a VCSEL light source. Biomed. Opt. Express 12, 3553. https://doi.org/10.1364/boe.425411.
Niederleithner, M., De Sisternes, L., Stino, H., Sedova, A., Schlegl, T., Bagherinia, H., Britten, A., Matten, P., Schmidt-Erfurth, U., Pollreisz, A., Drexler, W., Leitgeb, R.A., Schmoll, T., 2023. Ultra-widefield OCT angiography. IEEE Trans. Med. Imag. 42, 1009–1020. https://doi.org/10.1109/TMI.2022.3222638.
Nobre Cardoso, J., Keane, P.A., Sim, D.A., Bradley, P., Agrawal, R., Addison, P.K., Egan, C., Tufail, A., 2016. Systematic evaluation of optical coherence tomography angiography in retinal vein occlusion. Am. J. Ophthalmol. 163, 93–107.e6. https://doi.org/10.1016/j.ajo.2015.11.025.
Otani, T., Kishi, S., Maruyama, Y., 1999. Patterns of diabetic macular edema with optical coherence tomography. Am. J. Ophthalmol. 127, 688–693.
Parodi, M.B., Bandello, F., 2009. Branch retinal vein occlusion: classification and treatment. Ophthalmologica 223.
Parodi, M.B., Cicinelli, M.V., Rabiolo, A., Pierro, L., Gagliardi, M., Bolognesi, G., Bandello, F., 2017. Vessel density analysis in patients with retinitis pigmentosa by means of optical coherence tomography angiography. Br. J. Ophthalmol. 101, 428–432. https://doi.org/10.1136/bjophthalmol-2016-308925.
Pi, S., Hormel, T.T., Wei, X., Cepurna, W., Camino, A., Guo, Y., Huang, D., Morrison, J., Jia, Y., 2019. Monitoring retinal responses to acute intraocular pressure elevation in rats with visible light optical coherence tomography. Neurophotonics 6, 1. https://doi.org/10.1117/1.nph.6.4.041104.
Pi, S., Hormel, T.T., Wei, X., Cepurna, W., Wang, B., Morrison, J.C., Jia, Y., 2020. Retinal capillary oximetry with visible light optical coherence tomography. Proc. Natl. Acad. Sci. U. S. A. 117. https://doi.org/10.1073/pnas.1918546117.
Pichi, F., Salas, E.C., D De Smet, M., Gupta, V., Zierhut, M., Munk, M.R., 2021. Standardisation of optical coherence tomography angiography nomenclature in uveitis: first survey results. Br. J. Ophthalmol. 105, 941–947. https://doi.org/10.1136/bjophthalmol-2020-316881.
Pichi, F., Smith, S.D., Abboud, E.B., Neri, P., Woodstock, E., Hay, S., Levine, E., Baumal, C.R., 2020. Wide-field optical coherence tomography angiography for the detection of proliferative diabetic retinopathy. Graefe's Arch. Clin. Exp. Ophthalmol. 258, 1901–1909. https://doi.org/10.1007/s00417-020-04773-x.
Ploner, S.B., Kraus, M.F., Moult, E.M., Husvogt, L., Schottenhamml, J., Yasin Alibhai, A., Waheed, N.K., Duker, J.S., Fujimoto, J.G., Maier, A.K., 2021. Efficient and high accuracy 3-D OCT angiography motion correction in pathology. Biomed. Opt. Express 12, 125. https://doi.org/10.1364/boe.411117.
Poddar, R., Kim, D.Y., Werner, J.S., Zawadzki, R.J., 2014. In vivo imaging of human vasculature in the chorioretinal complex using phase-variance contrast method with phase-stabilized 1-μm swept-source optical coherence tomography. J. Biomed. Opt. 19. https://doi.org/10.1117/1.

Ponugoti, A., Baumal, C.R., Vajzovic, L., 2022. Optical coherence tomography angiography in pediatric retinal disorders. J Vitreoretin Dis. https://doi.org/10.1177/24741264221083873.
Potsaid, B., Baumann, B., Huang, D., Barry, S., Cable, A.E., Schuman, J.S., Duker, J.S., Fujimoto, J.G., 2010. Ultrahigh speed 1050nm swept source/Fourier domain OCT retinal and anterior segment imaging at 100,000 to 400,000 axial scans per second. Opt. Express 18, 20029–20048. https://doi.org/10.1364/OE.18.020029.
Potsaid, B., Jayaraman, V., Fujimoto, J.G., Jiang, J., Heim, P.J.S., Cable, A.E., 2012. MEMS tunable VCSEL light source for ultrahigh speed 60kHz - 1MHz axial scan rate and long range centimeter class OCT imaging. Optical Coherence Tomography and Coherence Domain Optical Methods in Biomedicine XVI, 82130M. https://doi.org/10.1117/12.911098. SPIE.
Prasad, P.S., Oliver, S.C.N., Coffee, R.E., Hubschman, J.P., Schwartz, S.D., 2010. Ultra wide-field angiographic characteristics of branch retinal and Hemicentral retinal vein occlusion. Ophthalmology 117, 780–784. https://doi.org/10.1016/j.ophtha.2009.09.019.
Pulido, J.S., Flaxel, C.J., Adelman, R.A., Hyman, L., Folk, J.C., Olsen, T.W., 2016. Retinal vein occlusions PPP. Ophthalmology 123, P182–P208. https://doi.org/10.1016/j.ophtha.2015.10.045.
Qian, Y., Yang, J., Liang, A., Zhao, C., Gao, F., Zhang, M., 2021. Widefield swept-source optical coherence tomography angiography assessment of choroidal changes in Vogt-Koyanagi-Harada disease. Front. Med. 8. https://doi.org/10.3389/fmed.2021.698644.
Quinn, N., Csincsik, L., Flynn, E., Curcio, C.A., Kiss, S., Sadda, S.V.R., Hogg, R., Peto, T., Lengyel, I., 2019. The clinical relevance of visualising the peripheral retina. Prog. Retin. Eye Res. https://doi.org/10.1016/j.preteyeres.2018.10.001.
Rebhun, C.B., Moult, E.M., Novais, E.A., Moreira-Neto, C., Ploner, S.B., Louzada, R.N., Lee, B., Baumal, C.R., Fujimoto, J.G., Duker, J.S., Waheed, N.K., Ferrara, D., 2017. Polypoidal choroidal vasculopathy on swept-source optical coherence tomography angiography with variable interscan time analysis. Transl. Vis. Sci. Technol. 6. https://doi.org/10.1167/tvst.6.6.4.
Remtulla, S., Hallett, P.E., 1985. A schematic eye for the mouse, and comparisons with the rat. Vis. Res. 25, 21–31. https://doi.org/10.1016/0042-6989(85)90076-8.
Robinson, R., Barathi, V.A., Chaurasia, S.S., Wong, T.Y., Kern, T.S., 2012. Update on animal models of diabetic retinopathy: from molecular approaches to mice and higher mammals. DMM Disease Models and Mechanisms. https://doi.org/10.1242/dmm.009597.
Rodrigues, M.M., Ballintine, E.J., Wiggert, B.N., Lee, L., Fletcher, R.T., Chader, G.J., 1984. Ocular pathology for clinicians choroideremia: a clinical, electron microscopic, and biochemical report. Ophthalmology 91.
Rudnik, N.D., Vingopoulos, F., Wang, J.C., Garg, I., Cui, Y., Zhu, Y., Le, R., Katz, R., Lu, Y., Patel, N.A., Miller, J.B., 2023. Characterising collateral vessels in eyes with branch retinal vein occlusions using widefield swept-source optical coherence tomography angiography. Br. J. Ophthalmol. 107.
Russell, J.F., Flynn, H.W., Sridhar, J., Townsend, J.H., Shi, Y., Fan, K.C., Scott, N.L., Hinkle, J.W., Lyu, C., Gregori, G., Russell, S.R., Rosenfeld, P.J., 2019a. Distribution of diabetic neovascularization on ultra-widefield fluorescein angiography and on simulated widefield OCT angiography. Am. J. Ophthalmol. 207, 110–120. https://doi.org/10.1016/j.ajo.2019.05.031.
Russell, J.F., Scott, N.L., Townsend, J.H., Shi, Y., Gregori, G., Crane, A.M., Flynn, H.W., Sridhar, J., Rosenfeld, P.J., 2021. Wide-field swept-source optical coherence tomography angiography of diabetic tractional retinal detachments before and after surgical repair. Retina 41, 1587–1596. https://doi.org/10.1097/IAE.0000000000003146.
Russell, J.F., Shi, Y., Hinkle, J.W., Scott, N.L., Fan, K.C., Lyu, C., Gregori, G., Rosenfeld, P.J., 2019b. Longitudinal wide-field swept-source OCT angiography of neovascularization in proliferative diabetic retinopathy after Panretinal photocoagulation. Ophthalmol Retina 3, 350–361. https://doi.org/10.1016/j.oret.2018.11.008.
Russell, J.F., Shi, Y., Scott, N.L., Gregori, G., Rosenfeld, P.J., 2020. Longitudinal angiographic evidence that intraretinal microvascular abnormalities can evolve into neovascularization. Ophthalmol Retina 4, 1146–1150. https://doi.org/10.1016/j.oret.2020.06.010.
Russell, J.F., Zhou, H., Shi, Y., Shen, M., Gregori, G., Feuer, W.J., Wang, R.K., Rosenfeld, P.J., 2022. Longitudinal analysis of diabetic choroidopathy in proliferative diabetic retinopathy treated with panretinal photocoagulation using widefield swept-source optical coherence tomography. Retina 42, 417–425. https://doi.org/10.1097/IAE.0000000000003375.
Sawada, O., Ichiyama, Y., Obata, S., Ito, Y., Kakinoki, M., Sawada, T., Saishin, Y., Ohji, M., 2018. Comparison between wide-angle OCT angiography and ultra-wide field fluorescein angiography for detecting non-perfusion areas and retinal neovascularization in eyes with diabetic retinopathy. Graefe's Arch. Clin. Exp. Ophthalmol. 256, 1275–1280. https://doi.org/10.1007/s00417-018-3992-y.
Scanlon, P.H., 2019. Diabetic retinopathy. Medicine (United Kingdom) 47, 77–85. https://doi.org/10.1016/j.mpmed.2018.11.013.
Schaal, K.B., Munk, M.R., Wyssmueller, I., Berger, L.E., Zinkernagel, M.S., Wolf, S., 2019. Vascular abnormalities in diabetic retinopathy assessed with swept-source optical coherence tomography angiography widefield imaging. Retina 39, 79–87. https://doi.org/10.1097/IAE.0000000000001938.
Schmidt-Erfurth, U., Sadeghipour, A., Gerendas, B.S., Waldstein, S.M., Bogunović, H., 2018. Artificial intelligence in retina. Prog. Retin. Eye Res. 67, 1–29. https://doi.org/10.1016/j.preteyeres.2018.07.004.
Schwartz, D.M., Fingler, J., Kim, D.Y., Zawadzki, R.J., Morse, L.S., Park, S.S., Fraser, S.E., Werner, J.S., 2014. Phase-variance optical coherence tomography: a technique for noninvasive angiography. Ophthalmology 121, 180–187. https://doi.org/10.1016/j.ophtha.2013.09.002.
Schwartz, R., Khalid, H., Sivaprasad, S., Nicholson, L., Anikina, E., Sullivan, P., Patel, P. J., Balaskas, K., Keane, P.A., 2020. Objective evaluation of proliferative diabetic retinopathy using OCT. In: Ophthalmology Retina. Elsevier Inc, pp. 164–174. https://doi.org/10.1016/j.oret.2019.09.004.
Seknazi, D., Coscas, F., Sellam, A., Rouimi, F., Coscas, G., Souied, E.H., Glacet-bernard, A., 2018. OPTICAL coherence tomography angiography in retinal vein occlusion correlations between macular vascular density, visual acuity, and peripheral nonperfusion area on fluorescein angiography. Retina 38.
Shields, J.A., Shields, C.L., Honavar, S.G., Demirci, H., Cater, J., 2001. Classification and Management of Coats Disease: The 2000 Proctor Lecture.
Shiraki, A., Sakimoto, S., Eguchi, M., Kanai, M., Hara, C., Fukushima, Y., Nishida, Kentaro, Kawasaki, R., Sakaguchi, H., Nishida, Kohji, 2022. Analysis of progressive neovascularization in diabetic retinopathy using widefield OCT angiography. In: Ophthalmology Retina. Elsevier Inc., pp. 153–160. https://doi.org/10.1016/j.oret.2021.05.011
Shiraki, A., Sakimoto, S., Tsuboi, K., Wakabayashi, T., Hara, C., Fukushima, Y., Sayanagi, K., Nishida, Kentaro, Sakaguchi, H., Nishida, Kohji, 2019. Evaluation of retinal nonperfusion in branch retinal vein occlusion using wide-field optical coherence tomography angiography. Acta Ophthalmol. 97, e913–e918. https://doi.org/10.1111/aos.14087.
Silva, P.S., Dela Cruz, A.J., Ledesma, M.G., Van Hemert, J., Radwan, A., Cavallerano, J. D., Aiello, L.M., Sun, J.K., Aiello, L.P., 2015. Diabetic retinopathy severity and peripheral lesions are associated with nonperfusion on ultrawide field angiography. Ophthalmology 122, 2465–2472. https://doi.org/10.1016/j.ophtha.2015.07.034.
Smith, L.E.H., Wesolowski, E., McLellan, A., Kostyk, S.K., D'Amato, R., Sullivan, R., D'Amore, P.A., 1994. Oxygen-induced retinopathy in the mouse. Investig. Ophthalmol. Vis. Sci. 35, 101–111.
Soliman, N., Mamdouh, D., Elkordi, A., 2023. Choroidal melanoma: a mini review. Medicines 10, 11. https://doi.org/10.3390/medicines10010011.
Song, P., Xu, Y., Zha, M., Zhang, Y., Rudan, I., 2019. Global epidemiology of retinal vein occlusion: a systematic review and meta-analysis of prevalence, incidence, and risk factors. J. Glob. Health 9. https://doi.org/10.7189/jogh.09.010427.
Spaide, R.F., Fujimoto, J.G., Waheed, N.K., Sadda, S.R., Staurenghi, G., 2018. Optical coherence tomography angiography. Prog. Retin. Eye Res. 64, 1–55. https://doi.org/10.1136/bjophthalmol-2016-309200.
Spaide, R.F., Lee, J.K., Klancnik, J.M., Gross, N.E., 2003. Optical coherence tomography of branch retinal vein occlusion. Retina.
Stino, H., Huber, K.L., Niederleithner, M., Mahnert, N., Sedova, A., Schlegl, T., Steiner, I., Sacu, S., Drexler, W., Schmoll, T., Leitgeb, R., Schmidt-Erfurth, U., Pollreisz, A., 2023. Association of diabetic lesions and retinal nonperfusion using widefield multimodal imaging. Ophthalmol Retina 7, 1042–1050. https://doi.org/10.1016/j.oret.2023.07.020.
Stino, H., Niederleithner, M., Iby, J., Sedova, A., Schlegl, T., Steiner, I., Sacu, S., Drexler, W., Schmoll, T., Leitgeb, R., Schmidt-Erfurth, U.M., Pollreisz, A., 2024. Detection of diabetic neovascularisation using single-capture 65°-widefield optical coherence tomography angiography. Br. J. Ophthalmol. 108, 91–97. https://doi.org/10.1136/bjo-2022-322134.
Su, J.P., Chandwani, R., Gao, S.S., Pechauer, A.D., Zhang, M., Wang, J., Jia, Y., Huang, D., Liu, G., 2016. Calibration of optical coherence tomography angiography with a microfluidic chip. J. Biomed. Opt. 21, 086015. https://doi.org/10.1117/1.jbo.21.8.086015.
SUPPORT Study Group of the Eunice Kennedy Shriver NICHD Neonatal Research Network, 2010. Target ranges of oxygen saturation in extremely preterm infants. N. Engl. J. Med. 362, 1959–1969. https://doi.org/10.1056/nejmoa0911781.
Swanson, E.A., Huang, D., 2011. Ophthalmic OCT Reaches $1Billion Per Year. Retin Physician, pp. 56–62.
Takagi, S., Hirami, Y., Takahashi, M., Fujihara, M., Mandai, M., Miyakoshi, C., Tomita, G., Kurimoto, Y., 2018. Optical coherence tomography angiography in patients with retinitis pigmentosa who have normal visual acuity. Acta Ophthalmol. 96, e636–e642. https://doi.org/10.1111/aos.13680.
Tan, B., McNabb, R.P., Zheng, F., Sim, Y.C., Yao, X., Chua, J., Ang, M., Hoang, Q.V., Kuo, A.N., Schmetterer, L., 2021. Ultrawide field, distortion-corrected ocular shape estimation with MHz optical coherence tomography (OCT). Biomed. Opt. Express 12, 5770. https://doi.org/10.1364/boe.428430.
Tang, W., Guo, J., Liu, W., Xu, G., 2020. Optical coherence tomography angiography of inflammatory choroidal neovascularization early response after anti-VEGF treatment. Curr. Eye Res. 45, 1556–1562. https://doi.org/10.1080/02713683.2020.1767790.
Tian, M., Tappeiner, C., Zinkernagel, M.S., Huf, W., Wolf, S., Munk, M.R., 2019. Evaluation of vascular changes in intermediate uveitis and retinal vasculitis using swept-source wide-field optical coherence tomography angiography. Br. J. Ophthalmol. 103, 1289–1295. https://doi.org/10.1136/bjophthalmol-2018-313078.
Ting, D.S.W., Cheung, G.C.M., Wong, T.Y., 2016. Diabetic retinopathy: global prevalence, major risk factors, screening practices and public health challenges: a review. Clin. Exp. Ophthalmol. https://doi.org/10.1111/ceo.12696.
Toto, L., Borrelli, E., Mastropasqua, R., Senatore, A., Di Antonio, L., Di Nicola, M., Carpineto, P., Mastropasqua, L., 2016. Macular features in retinitis pigmentosa: correlations among ganglion cell complex thickness, capillary density, and macular function. Investig. Ophthalmol. Vis. Sci. 57, 6360–6366. https://doi.org/10.1167/iovs.16-20544.
Tozburun, S., Siddiqui, M., Vakoc, B.J., 2014. A rapid, dispersion-based wavelength-stepped and wavelength-swept laser for optical coherence tomography. Opt. Express 22, 3414. https://doi.org/10.1364/oe.22.003414.
Tsuboi, K., Mazloumi, M., Guo, Y., Wang, J., Flaxel, C.J., Bailey, S.T., Huang, D., Jia, Y., Hwang, T.S., 2023. Utility of en face OCT for the detection of clinically unsuspected

retinal neovascularization in patients with diabetic retinopathy. Ophthalmol Retina 1–9. https://doi.org/10.1016/j.oret.2023.03.002.
Tsuboi, K., Mazloumi, M., Guo, Y., Wang, J., Flaxel, C.J., Bailey, S.T., Wilson, D.J., Huang, D., Jia, Y., Hwang, T.S., 2024. Early sign of retinal neovascularization evolution in diabetic retinopathy: a longitudinal OCT angiography study. Ophthalmology Science 4. https://doi.org/10.1016/j.xops.2023.100382.
Vaquer, G., Riviere Dannerstedt, F., Mavris, M., Bignami, F., Llinares-Garcia, J., Westermark, K., Sepodes, B., 2013. Animal models for metabolic, neuromuscular and ophthalmological rare diseases. Nat. Rev. Drug Discov. 12.
Varshney, N., Kebede, A.A., Owusu-Dapaah, H., Lather, J., Kaushik, M., Bhullar, J.S., 2017. A review of von Hippel-Lindau syndrome. J Kidney Cancer VHL 4, 20–29. https://doi.org/10.15586/jkcvhl.2017.88.
Vaz-Pereira, S., Dansingani, K.K., Chen, K.C., Cooney, M.J., Klancnik, J.M., Engelbert, M., 2017. Tomographic relationships between retinal neovascularization and the posterior vitreous in proliferative diabetic retinopathy. Retina 37, 1287–1296. https://doi.org/10.1097/IAE.0000000000001336.
Vergnole, S., Lévesque, D., Lamouche, G., 2010. Experimental validation of an optimized signal processing method to handle non-linearity in swept-source optical coherence tomography. https://doi.org/10.1364/OA_License_v1#VOR.
Wang, C., Yin, Z., He, B., Chen, Z., Hu, Z., Shi, Y., Zhang, X., Zhang, N., Jing, L., Wang, G., Xue, P., 2023a. Polarization-isolated stretched-pulse mode-locked swept laser for 10.3-MHz A-line rate optical coherence tomography. Opt Lett 48, 4025. https://doi.org/10.1364/ol.495786.
Wang, J., Camino, A., Hua, X., Lku, L., Huang, D., Hwang, T.S., Jia, Y., 2019. Invariant features-based automated registration and montage for wide-field OCT angiography. Biomed. Opt. Express 10, 120–136. https://doi.org/10.1364/boe.10.000120.
Wang, J., Hormel, T.T., Jia, Y., 2022. Artificial intelligence-assisted projection-resolved optical coherence tomographic angiography (aiPR-OCTA). Investig. Ophthalmol. Vis. Sci. 63.
Wang, J., Hormel, T.T., Tsuboi, K., Wang, X., Ding, X., Peng, X., Huang, D., Bailey, S.T., Jia, Y., 2023b. Deep learning for diagnosing and segmenting choroidal neovascularization in OCT angiography in a large real-world data set. Transl. Vis. Sci. Technol. 12, 15. https://doi.org/10.1167/tvst.12.4.15.
Wei, X., Camino, A., Pi, S., Guo, Y., Jian, Y., Huang, D., Jia, Y., 2019a. A novel and effective scan pattern for velocimetric OCT angiography. In: Izatt, J.A., Fujimoto, J. G. (Eds.), Optical Coherence Tomography and Coherence Domain Optical Methods in Biomedicine, vol. XXIII, p. 20. https://doi.org/10.1117/12.2510653. SPIE.
Wei, X., Camino, A., Pi, S., Hormel, T.T., Cepurna, W., Huang, D., Morrison, J.C., Jia, Y., 2019b. Real-time cross-sectional and en face OCT angiography guiding high-quality scan acquisition. Opt Lett 44, 1431. https://doi.org/10.1364/ol.44.001431.
Wei, X., Hormel, T.T., Guo, Y., Hwang, T.S., Jia, Y., 2020. High-resolution wide-field OCT angiography with a self-navigation method to correct microsaccades and blinks. Biomed. Opt. Express 11, 3234. https://doi.org/10.1364/boe.390430.
Wei, X., Hormel, T.T., Guo, Y., Jia, Y., 2019c. 75-degree non-mydriatic single-volume optical coherence tomographic angiography. Biomed. Opt. Express 10, 6286–6295.
Wei, X., Hormel, T.T., Jia, Y., 2021. Phase-stabilized complex-decorrelation angiography. Biomed. Opt. Express 12, 2419–2431.
Wei, X., Hormel, T.T., Pi, S., Guo, Y., Jian, Y., Jia, Y., 2019d. High dynamic range optical coherence tomography angiography (HDR-OCTA). Biomed. Opt. Express 10, 3560. https://doi.org/10.1364/boe.10.003560.
Wei, X., Hormel, T.T., Renner, L., Neuringer, M., Jia, Y., 2024. Wide-field OCT angiography for non-human primate retinal imaging. Biomed. Opt. Express 15, 4642. https://doi.org/10.1364/boe.525839.
Westphal, Volker Rollins, Andrew, M., Radhakrishnan, Sunita, Izatt, Joseph A., Drexler, W., Morgner, U., Ghanta, R.K., Kartner, F.X., Schuman, J.S., Fujimoto, J.G., Radhakrishnan, S., Rollins, A.M., Roth, J.E., Yazdanfar, S., Westphal, V., Bardenstein, D.S., Izatt, J.A., Ung-arunyawee, R., Chak, A., K Wong, R.C., Kobayashi, K., Sivak, M.V., 2000. Correction of geometric and refractive image distortions in optical coherence tomography applying Fermat's principle. Skin Res. Technol. https://doi.org/10.1364/OA_License_v1#VOR.
Wieser, W., Biedermann, B.R., Klein, T., Eigenwillig, C.M., Huber, R., 2010. Multi-Megahertz OCT: high quality 3D imaging at 20 million A-scans and 45 GVoxels per second. Opt. Express 18, 14685–14704. https://doi.org/10.1364/OE.18.014685.
Wojtkowski, M., Kowalczyk, a, Leitgeb, R., Fercher, a F., 2002. Full range complex spectral optical coherence tomography technique in eye imaging. Opt Lett 27, 1415–1417. https://doi.org/10.1364/OL.27.001415.
Wollstein, G., Kagemann, L., Bilonick, R.A., Ishikawa, H., Folio, L.S., Gabriele, M.L., Ungar, A.K., Duker, J.S., Fujimoto, J.G., Schuman, J.S., 2012. Retinal nerve fibre layer and visual function loss in glaucoma: the tipping point. Br. J. Ophthalmol. 96, 47–52. https://doi.org/10.1136/bjo.2010.196907.
Wong, W.T., Agrón, E., Coleman, H.R., Tran, T., Reed, G.F., Csaky, K., Chew, E.Y., 2008. Clinical Characterization of Retinal Capillary Hemangioblastomas in a Large Population of Patients with von Hippel-Lindau Disease. Ophthalmology 115, 181–188. https://doi.org/10.1016/j.ophtha.2007.03.009.
Xi, J., Li, J., Li, X., 2010. Generic real-time uniform K-space sampling method for high-speed swept-Source optical coherence tomography. Opt. Express 11, 2183–2189. https://doi.org/10.1364/OA_License_v1#VOR.
Xiong, H., You, Q.S., Guo, Y., Wang, J., Wang, B., Gao, L., Flaxel, C.J., Bailey, S.T., Hwang, T.S., Jia, Y., 2021. Deep learning-based signal-independent assessment of macular avascular area on 6×6 mm optical coherence tomography angiogram in diabetic retinopathy: a comparison to instrument-embedded software. Br. J. Ophthalmol. https://doi.org/10.1136/bjophthalmol-2020-318646 bjophthalmol-2020-318646.
Xu, J., Wong, K., Jian, Y., Sarunic, M.V., 2014. Real-time acquisition and display of flow contrast using speckle variance optical coherence tomography in a graphics processing unit. J. Biomed. Opt. 19, 1. https://doi.org/10.1117/1.jbo.19.2.026001.
Xu, K., Tzankova, V., Li, C., Sharma, S., 2016. Intravenous fluorescein angiography–associated adverse reactions. Can. J. Ophthalmol. 51, 321–325. https://doi.org/10.1016/j.jcjo.2016.03.015.
Yang, J., Liu, L., Campbell, J.P., Huang, D., Liu, G., 2017a. Handheld optical coherence tomography angiography. Biomed. Opt. Express 8, 2287. https://doi.org/10.1364/boe.8.002287.
Yang, J., Su, J., Wang, J., Men, S., Jia, Y., Huang, D., Liu, G., 2017b. Hematocrit dependence of flow signal in optical coherence tomography angiography. Biomed. Opt. Express 8, 776. https://doi.org/10.1364/boe.8.000776.
Yang, P., Ohno, S., Zierhut, M., 2021. Editorial: new insights into uveitis: immunity, genes, and microbes. Front. Immunol. 12. https://doi.org/10.3389/fimmu.2021.765377.
Yang, P., Zhang, Z., Zhou, H., Li, B., Huang, X., Gao, Y., Zhu, L., Ren, Y., Klooster, J., Kijlstra, A., 2005. Clinical patterns and characteristics of uveitis in a tertiary center for uveitis in China. Curr. Eye Res. 30. https://doi.org/10.1080/02713680500263606?scroll=top&needAccess=true.
Yao, X., Toslak, D., Son, T., Ma, J., 2021. Understanding the relationship between visual-angle and eye-angle for reliable determination of the field-of-view in ultra-wide field fundus photography. Biomed. Opt. Express 12, 6651. https://doi.org/10.1364/boe.433775.
Yasuno, Y., Hong, Y., Makita, S., Yamanari, M., Akiba, M., Miura, M., Yatagai, T., 2007. In vivo high-contrast imaging of deep posterior eye by 1-μm swept source optical coherence tomography and scattering optical coherence angiography. Opt. Express 15, 6121. https://doi.org/10.1364/OA_License_v1#VOR.
You, Q.S., Guo, Y., Wang, J., Wei, X., Camino, A., Zang, P., Flaxel, C.J., Bailey, S.T., Huang, D., Jia, Y., Hwang, T.S., 2019. Detection of clinically unsuspected retinal neovascularization with wide-field optical coherence tomography angiography. Retina 00 1. https://doi.org/10.1097/iae.0000000000002487.
Zahid, S., Chen, K.C., Jung, J.J., Balaratnasingam, C., Ghadiali, Q., Sorenson, J., Rofagha, S., Freund, K.B., Yannuzzi, L.A., 2017. Optical coherence tomography angiography of chorioretinal lesions due to idiopathic multifocal choroiditis. Retina 37, 1451–1463. https://doi.org/10.1097/IAE.0000000000001381.
Zang, P., Hormel, T.T., Hwang, T.S., Bailey, S.T., Huang, D., Jia, Y., 2023. Deep-learning–aided diagnosis of diabetic retinopathy, age-related macular degeneration, and glaucoma based on structural and angiographic OCT. Ophthalmology Science 3, 100245. https://doi.org/10.1016/j.xops.2022.100245.
Zang, P., Hormel, T.T., Wang, X., Tsuboi, K., Huang, D., Hwang, T.S., Jia, Y., 2022. A diabetic retinopathy classification framework based on deep-learning analysis of OCT angiography. Transl. Vis. Sci. Technol. 11, 1–13. https://doi.org/10.1167/tvst.11.7.10.
Zang, P., Liu, G., Zhang, M., Dongye, C., Wang, J., Pechauer, A.D., Hwang, T.S., Wilson, D.J., Huang, D., Li, D., Jia, Y., 2016. Automated motion correction using parallel-strip registration for wide-field en face OCT angiogram. Biomed. Opt. Express 7, 2823. https://doi.org/10.1364/boe.7.002823.
Zang, P., Liu, G., Zhang, M., Wang, J., Hwang, T.S., Wilson, D.J., Huang, D., Li, D., Jia, Y., 2017. Automated three-dimensional registration and volume rebuilding for wide-field angiographic and structural optical coherence tomography. J. Biomed. Opt. 22, 026001. https://doi.org/10.1117/1.jbo.22.2.026001.
Zhang, J., Jung, W., Nelson, J.S., Chen, Z., 2004. Full range polarization-sensitive Fourier domain optical coherence tomography. Opt. Express 24, 1178–1181. https://doi.org/10.1364/OA_License_v1#VOR.
Zhang, J., Nguyen, T., Potsaid, B., Jayaraman, V., Burgner, C., Chen, S., Li, J., Liang, K., Cable, A., Traverso, G., Mashimo, H., Fujimoto, J.G., 2021. Multi-MHz MEMS-VCSEL swept-source optical coherence tomography for endoscopic structural and angiographic imaging with miniaturized brushless motor probes. Biomed. Opt. Express 12, 2384. https://doi.org/10.1364/boe.420394.
Zhang, Q., Huang, Y., Zhang, T., Kubach, S., An, L., Laron, M., Sharma, U., Wang, R.K., 2015. Wide-field imaging of retinal vasculature using optical coherence tomography-based microangiography provided by motion tracking. J. Biomed. Opt. 20, 066008. https://doi.org/10.1117/1.jbo.20.6.066008.
Zhang, Q., Lee, C.S., Chao, J., Chen, C.-L., Zhang, T., Sharma, U., Zhang, A., Liu, J., Rezaei, K., Pepple, K.L., Munsen, R., Kinyoun, J., Johnstone, M., Van Gelder, R.N., Wang, R.K., 2016. Wide-field optical coherence tomography based microangiography for retinal imaging. Sci. Rep. 6, 22017. https://doi.org/10.1038/srep22017.
Zhi, Z., Cepurna, W., Johnson, E., Jayaram, H., Morrison, J., Wang, R.K., 2015. Evaluation of the effect of elevated intraocular pressure and reduced ocular perfusion pressure on retinal capillary bed filling and total retinal blood flow in rats by OMAG/OCT. Microvasc. Res. 101, 86–95. https://doi.org/10.1016/j.mvr.2015.07.001.
Zhi, Z., Cepurna, W.O., Johnson, E.C., Morrison, J.C., Wang, R.K., 2012. Impact of intraocular pressure on changes of blood flow in the retina, choroid, and optic nerve head in rats investigated by optical microangiography. Biomed. Opt. Express 3, 2220–2233. https://doi.org/10.1364/BOE.3.002220.
Zitová, B., Flusser, J., 2003. Image registration methods: a survey. Image Vis Comput. 21, 977–1000. https://doi.org/10.1016/S0262-8856(03)00137-9.